processes

Article

Performance, Combustion, and Emission Comparisons of a High-Speed Diesel Engine Fueled with Biodiesel with Different Ethanol Addition Ratios Based on a Combined Kinetic Mechanism

Yunhao Zhong [1], Yanhui Zhang [1], Chengfang Mao [1,2,*] and Ananchai Ukaew [2]

1 School of Mechanical and Automotive Engineering, Guangxi University of Science and Technology, Liuzhou 545006, China
2 Faculty of Engineering, Naresuan University, Phitsanulok 65000, Thailand
* Correspondence: 100001935@gxust.edu.cn

Abstract: In this work, different ethanol ratios (5%, 10%, 15%, and 20%) blended with biodiesel were used to investigate the effects of ethanol addition on engine performance, combustion, and emission characteristics of a high-speed diesel engine in terms of brake power, brake specific fuel consumption, brake thermal efficiency, cylinder pressure, cylinder temperature, heat release rate, NOx, CO, and soot emissions. First, a three-dimensional CFD model was established by AVL-Fire combined with the CHEMKIN code. Then, an improved kinetic mechanism with 430 reactions and 122 species was developed by combining a three-component biodiesel combustion mechanism and ethanol mechanism to accurately simulate the blended fuel combustion processes. The results indicated that compared with biodiesel, the maximum brake specific fuel consumption increased by 6.08%, and the maximum brake thermal efficiency increased by 2.09% for the blended fuel. In addition, NO_x and CO emissions for EE20 were reduced by 29.32% and 39.57% at full engine load. Overall, the ethanol addition can significantly decrease pollution emissions.

Keywords: diesel engine; ethanol addition; combustion; performance; emissions

check for updates

Citation: Zhong, Y.; Zhang, Y.; Mao, C.; Ukaew, A. Performance, Combustion, and Emission Comparisons of a High-Speed Diesel Engine Fueled with Biodiesel with Different Ethanol Addition Ratios Based on a Combined Kinetic Mechanism. *Processes* **2022**, *10*, 1689. https://doi.org/10.3390/pr10091689

Academic Editor: Jiaqiang E

Received: 3 August 2022
Accepted: 23 August 2022
Published: 25 August 2022

1. Introduction

In recent decades, fossil fuels have been the dominant energy source for aviation, stationary power generators, and automobiles [1]. Fossil fuels are becoming increasingly scarce because they are non-renewable and overexploited by humans [2]. According to the IEA (International Energy Agency), the energy consumption rate will reach 53% by 2030 [3]. Therefore, the depletion of fossil fuels will soon be apparent. To meet the needs of environmental and resource issues, many research institutions and scholars are looking for clean and high-efficiency alternative energy sources to replace fossil fuels [4].

Among the replacements for fossil fuels in the energy industry, biodiesel is a developing trend because it is sulfur-free, non-toxic, biodegradable, and reliable [5]. Moreover, due to the similar physicochemical properties, biodiesel can be directly used in a conventional diesel engine with little modification, and significantly reduce PM, HC, CO, and soot emissions [6,7]. In addition, biodiesel produced from vegetable oil, especially rapeseed oil, is environmentally friendly [8,9], and China is the world's largest producer and consumer of rapeseed oil [10]. Therefore, rapeseed biodiesel has expansive prospects for further development in the 21st century [11].

As described, biodiesel has superior advantages and should be defined as clean energy. Compared to fossil diesel, the lower PM, CO, and HC emissions of biodiesel lead to more significant potential use in diesel engines. However, the composition and properties of biodiesel are different from fossil diesel. Thus, some inferior properties of biodiesel, such as higher viscosity, density, lower volatility, and poor cold flow properties, will restrict the use of biodiesel in diesel engines [12]. A practical solution is to add some additives to biodiesel. In the production process of biodiesel, alcohol fuels such as methanol and ethanol were used as a catalyzer in the transesterification process for biodiesel production. Moreover, ethanol is also a biofuel that is gaining extensive attention from researchers [13]. It can be blended with biodiesel at different ratios and significantly improve biodiesel's characteristics. A study showed that ethanol as an additive by 30% volume concentration in palm biodiesel increased the ignition delay and burn-rate constant by up to 38.6% and 23.2%, respectively, whereas the evaporation duration and burning period decreased by up to 20.6% and 22.5%, respectively [14]. Overall, blending oxygenated compounds into biodiesel is considered an effective way to improve thermal efficiency and has the potential to achieve ultra-low CO and PM emissions in diesel engines.

Several studies also investigated the effects of oxygen additives such as methanol, ethanol, and n-butanol blended with diesel or biodiesel on engine performance and exhaust emissions. Aydin et al. [15] studied the effects of 20% ethanol addition to sunflower biodiesel (BE20) in a single-cylinder, four-strokes direct injection diesel engine. They observed that the average engine torque increased by 1.2% due to oxygen enrichment and more efficient lubricity of ethanol addition. Moreover, the brake thermal efficiency of BE20 blended fuel increased by 3.58% compared to fossil diesel. Adding ethanol and biodiesel increased NO_x emission but reduced CO and CO_2 emissions compared to diesel. Yilmaz et al. [16] carried out an experimental study in a diesel engine fueled with biodiesel-ethanol and biodiesel-methanol blends and investigated the engine performance and emission characteristics. Compared with methanol addition, ethanol addition is more effective for emission reduction.

Zheng et al. [17] compared the effects of three different oxygen additives, n-butanol (Bu20), ethanol (E20), and 2,5-dimethylfuran (DMF20), on the combustion and emission characteristics of a diesel engine fueled with biodiesel. The results indicated that the indicated thermal efficiency (ITE) of pure biodiesel and three blends were lower than that of diesel at low load. With the increase in load, three blends and pure biodiesel presented higher ITE than fossil diesel, especially at high EGR rates. Furthermore, compared with other oxygen additives, ethanol is more effective in decreasing NO_x and soot emissions. NO_x emission for E20 was lower than diesel while it was higher than other blends. Moreover, lower HC and CO emissions were also observed for the three fuel blends. Therefore, ethanol is a suitable biodiesel oxygen additive for diesel engines fueled with biodiesel compared with n-butanol, methanol, and 2,5-dimethylfuran [18].

Several studies were conducted to investigate the effect of ethanol addition on combustion and emission characteristics. Biswas et al. [19] investigated the effects of ethanol-blended Mahua biodiesel and spilled injection coupled Port Fuel Injection (PFI) on the performance, combustion, and emission characteristics of a diesel engine. The results indicated that with the addition of ethanol, the lower value of NO_x had been recorded for 10% pilot injection fuel percentage at 15–45° and −23° BTDC pilot main injection. Zhu et al. investigated the combustion, performance, and emission characteristics of diesel engine fueled with diesel, biodiesel, and biodiesel with 5%, 10%, and 15% ethanol and found a similar trend [20]. For emissions, the ethanol addition had the lower NO_x, PM, CO, and HC emissions than diesel. The ethanol addition can reduce the pollution emissions such as NO_x and PM. However, with the increase in ethanol ratios, the incomplete combustion product such as CO and HC could be increased due to the low heating value of ethanol.

Furthermore, Wu et al. [21] investigated the effects of different ethanol addition on a diesel engine fueled with palm oil biodiesel at idling speed. The results indicated that ethanol additives had an attenuation effect on CO, especially smoke emissions. The maximum smoke reduction is 71% for the blended fuel with 15 vol% ethanol. In addition, the smoke reduction increased with the increases of engine load. Gawale et al. [22] conducted a comparative study of ethanol-diesel and ethanol-biodiesel on a dual fuel mode homogeneous charge compression ignition (HCCI) engine for different engine loads. The results indicated that compared with ethanol-diesel dual mode, the ethanol-biodiesel could significantly reduce HC, smoke, and CO emissions. Moreover, for the HCCI engine, ethanol can replace diesel fuel with low NO_x, low smoke opacity, and better fuel economy. As for higher ethanol addition to biodiesel, Jiang et al. [23] investigated the effect of biodiesel with 40% ethanol on the electrospray and combustion and emissions characteristics in a mesoscale combustor. The results indicated that 40% ethanol to biodiesel reduced the droplet size thus decreasing CO emission.

Several experimental studies were carried out in the literature and it was evident that with the addition of ethanol, some pollution emissions had been decreased; however, to investigate the pressure, flow field, temperature, composition, and turbulence in the in-cylinder distribution, the numerical simulation has obvious advantages and is regarded as a very effective tool for saving energy and cost through detailed mechanisms [24]. For example, Zhang et al. [25] used an improved chemical kinetics mechanism with 134 species and 475 reactions to investigate the boiling heat transfer on the engine performance enhancement of a medium speed marine diesel engine fueled with biodiesel. The results indicated that the improved consideration of the boiling heat transfer model agreed better with the experiment result. Yang et al. [26] used the KIVA4 coupled with the CHEMKIN II code to investigate the biodiesel-methanol engine performance and emission characteristics. The results indicated that the simulations agreed well with the experimental study and some combustion characteristics and pollutant distribution were revealed through the code.

An et al. [27] used a skeletal reaction mechanism (SRM) to investigate the effects of ethanol addition on combustion characteristic of a diesel engine at a fixed engine speed of 2400 rpm and under 10%, 50%, and 100% load conditions. The results indicated that the SRM fit well in the experimental study. The CO and NO_x emissions generally decreased with the increased ethanol addition ratio. A similar trend was also observed by Yilmaz et al. [28] in an experimental study. Datta et al. [29] evaluated the performance, combustion, and emission characteristics of a diesel engine fueled with different ethanol-biodiesel blends. They also indicated that the simulations agreed with the experimental study and found an effective reduction in NO_x emissions with biodiesel and ethanol blends. Asadi et al. [30] numerically investigated the behavior of ethanol and biodiesel, blended with diesel fuel on a multiple injection diesel engine. The results also indicated that ethanol combustion resulted in lower chamber temperature and lower NO_x emission.

As was mentioned, the ethanol addition to biodiesel can significantly reduce the formation of polluting gases. To improve the combustion and emission characteristic of a diesel engine, the proper ethanol addition to biodiesel is very important. Therefore, in this paper, the AVL-Boost coupling with AVL-fire software and combined with CHEMKIN code were used to simulate the combustion process. First, a whole diesel engine model and part of the cylinder model were developed by AVL-Boost and AVL-fire according to the 4JB-1CN diesel engine. Then, the built model was validated by experimental results under 100%, 50%, and 25% load conditions at the speed of 1800 rpm. Finally, the combustion process, engine performance, and emission characteristics of different ethanol addition to biodiesel were simulated and compared using a skeletal mechanism of a combined mechanism with 430 reactions and 122 species. The findings are attractive due to the ethanol's influence on engine performance and emission reduction using different percentages.

2. Numerical Approaches

2.1. Model Set-Up and Calibration

In this paper, the combustion cylinder geometry was established using AVL-fire ESE diesel software and following these steps. First, the sketcher tools to create the piston bowl shape, fuel injector and input the shape parameters, block structure, and define boundary conditions. Then, in the Mesher section, check the number of boundary layers and thickness of boundary layers, and edit the dependent average cell size to generate high-quality hexahedral-based orthogonal meshes. Finally, save the meshes and import the meshes to the Fire workflow manager.

Figure 1 shows the whole coupling process of one-dimensional calculation and three-dimensional calculation. As shown in Figure 1, some boundary conditions of the three-dimensional calculation diesel engine model which were not measured by the experiment were obtained by the validated one-dimensional calculation model.

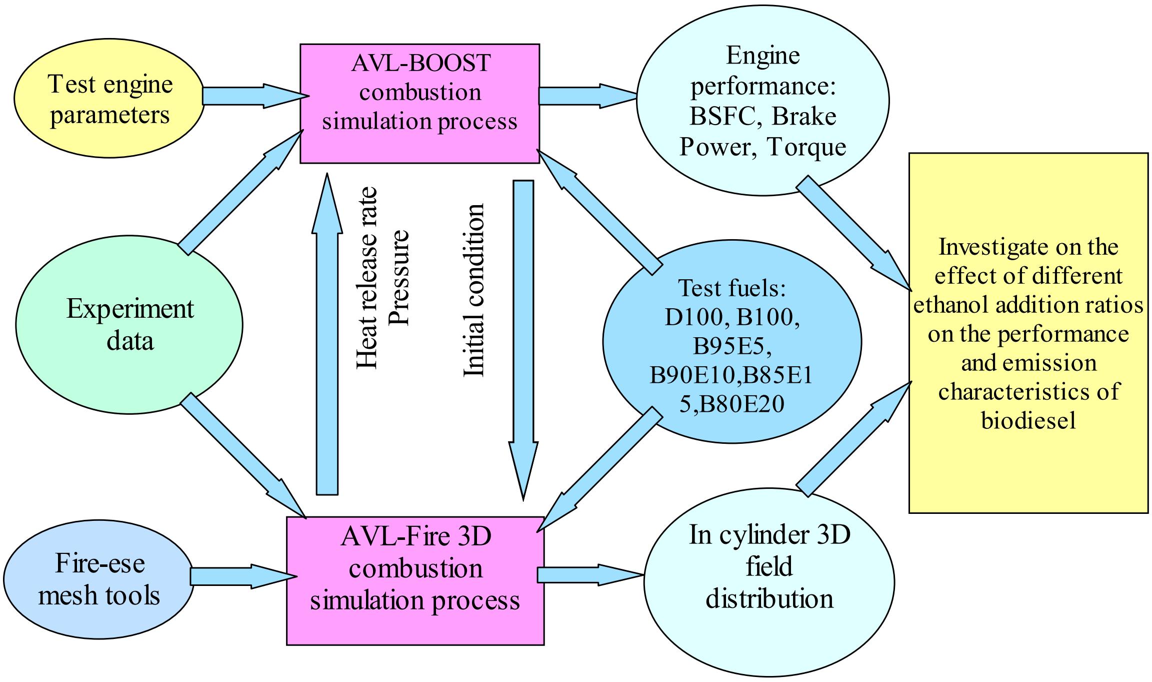

Figure 1. Coupling process of one-dimensional and three-dimensional calculation [1].

2.1.1. 1-D Simulation Model Validation and Calibration

The AVL-Boost was used to determine the boundary conditions which were not measured by the experiment, such as intake opening crank angle, exhaust closing crank angle, initial cylinder pressure, temperature, and creating the whole diesel engine. The one-dimensional model building and calibration processes are omitted here, and the specific construction process can be found in the previous work [25].

2.1.2. 3-D Simulation Model Validation and Calibration

The fluid flow process is controlled by the conservation equation. The material flow process in the internal combustion engine cylinder not only needs to follow the basic conservation equation, but also the component conservation equation. The equations of the AVL-Fire solve the momentum, energy, three-dimensional transient conservation equations of mass, turbulent fluid flow, and species are as follows:

(1) Mass Conservation Equation

$$\frac{\partial \rho}{\partial t} + \frac{\partial(\partial \rho i)}{\partial x} + \frac{\partial(\partial \rho j)}{\partial y} + \frac{\partial(\rho k)}{\partial z} = 0 \quad (1)$$

where ρ is the flow material density, g/cm^3; t is time, s; i, j, and k are velocity vectors in the x, y, and z directions, respectively.

(2) Momentum Conservation Equation

$$\frac{\partial(\rho i)}{\partial t} + div(\rho i U) = div(\mu grad i) - \frac{\partial p}{\partial x} \quad (2)$$

$$\frac{\partial(\rho j)}{\partial t} + div(\rho j U) = div(\mu grad j) - \frac{\partial p}{\partial y} \quad (3)$$

$$\frac{\partial(\rho k)}{\partial t} + div(\rho k U) = div(\mu gradk) - \frac{\partial p}{\partial z} \tag{4}$$

where μ is the hydrodynamic viscosity, Pa·s; U is the velocity vectors, m/s; *div* is an abbreviation for divergence, which indicates the calculation of the divergence of a vector; *grad* is an abbreviation for gradient, which indicates that the directional derivative of a function at this point takes the maximum value along this direction.

(3) Energy Conservation Equation

$$\frac{\partial(\rho T)}{\partial t} + div(\rho \overline{u} T) = div(\frac{k}{c_p} gradT) - \frac{\partial p}{\partial x} + S_h \tag{5}$$

where c_p is the constant pressure specific heat capacity, J/(kg·k); T is the temperature, k; k is the fluid heat transfer, W/(m^2·k); S_h is the released chemical energy, J.

(4) Component Conservation Equation

$$\frac{\partial(\rho Y_m)}{\partial t} + div(\rho u Y_m) = div(D_m grad(\rho Y_m)) + S_m \tag{6}$$

where Y_m is the mass fraction of component m; D_m is the diffusion coefficient; S_m is the source term of chemical reaction mass.

2.2. Simulation Mathematical Model

In this paper, the ethanol/biodiesel fuel combine mechanism was prepared using a combination of ethanol mechanism and biodiesel mechanism. This combination mechanism was widely used to simulation the combustion process of the diesel engine. Furthermore, in order to simulate the fuel spray, evaporation, atomization, combustion, and in-cylinder flow of the engine, suitable models need to choose and represent the engine combustion process.

2.2.1. Turbulence Model

In this paper, the in-cylinder fluid flow simulation was carried out in AVL-Fire environment and used a four-equation k-ζ-f turbulence model, which was widely used in diesel engine simulation due to its robustness [31]. The formula for calculating turbulent viscosity is:

$$v_t = C_\mu \zeta \frac{k^2}{\varepsilon} \tag{7}$$

$$\zeta = \frac{\overline{v^2}}{k} \tag{8}$$

where v_t is the turbulent viscosity, m^2/s; C_μ is the empirical constant, k is the turbulent kinetic energy, m^2/s^2; v is the velocity, m/s; ζ is the velocity scale ratio, ε is the turbulent kinetic energy dissipation rate. The k-ζ-f transport equations are as follows:

$$\rho\frac{Dk}{Dt} = \rho(P_k - \varepsilon) + \frac{\partial}{\partial x_j}\left[\left(\mu + \frac{\mu_t}{\sigma_k}\right)\frac{\partial k}{\partial x_j}\right] \tag{9}$$

$$\rho\frac{D\varepsilon}{Dt} = \rho\frac{C^*_{\varepsilon 1} P_k - C_{\varepsilon 2}\varepsilon}{T} + \frac{\partial}{\partial x_j}\left[\left(\mu + \frac{\mu_t}{\sigma_k}\right)\frac{\partial \varepsilon}{\partial x_j}\right] \tag{10}$$

$$\rho\frac{D\zeta}{Dt} = \rho f - \rho\frac{\zeta}{k} p_k + \frac{\partial}{\partial x_j}\left[\left(\mu + \frac{\mu_t}{\sigma_\zeta}\right)\frac{\partial \zeta}{\partial x_j}\right] \tag{11}$$

$$f - L^2\frac{\partial^2 f}{\partial x_j \partial x_j} = \left(C_1 + C_2\frac{P_k}{\zeta}\right)\frac{(2/3 - \zeta)}{T} \tag{12}$$

$$C^*_{\varepsilon 1} = C_{\varepsilon 1}\left(1 + 0.045\sqrt{1/\zeta}\right) \tag{13}$$

where P_k is the turbulent kinetic energy generation term, T is the turbulence time length, L is the turbulence scale length, $C_{\varepsilon 1}^{*}$ is the correction factor, $C_{\varepsilon 1}$, $C_{\varepsilon 2}$, C_1, and C_2 are empirical constants, f is the elliptic relaxation function.

2.2.2. Spray Model

The fuel injection process of a diesel engine is a complex process of gas flow and mutual mixing. The injection process includes fuel atomization, evaporation, oil mist mixing, and oil droplets hitting the wall. Therefore, it is necessary to comprehensively consider the conservation equations including gas and liquid phases in the process of simulating gas flow. In this paper, the trajectory and velocity equation of the oil droplets are as follows:

(1) Basic Momentum Equation

$$m_d \frac{du_{id}}{dt} = F_{idr} + F_{ig} + F_{ip} + F_{ib} \tag{14}$$

where m_d is the droplet mass, g; u_{id} is the oil droplet velocity vector; F_{idr} is the resistance, N; it can be calculated as:

$$F_{idr} = D_p \times U_{irel} \tag{15}$$

where D_p is the resistance function; it is defined as the following formula:

$$D_p = \frac{1}{2} \rho_g A_d C_d |U_{rel}| \tag{16}$$

where U_{rel} is the gas-liquid relative velocity, m/s; ρ_g is the gaseous density, kg/m^3; A_d is the representative area of the oil droplet, m^2; C_d is the drag coefficient, which is related to the droplet Reynolds number, and its specific functional relationship is as follows:

$$C_d \begin{cases} \frac{24}{\mathrm{Re}_d}\left(1 + 0.15\mathrm{Re}_d^{0.687}\right) & (\mathrm{Re}_d < 10^3) \\ 0.44 & (\mathrm{Re}_d \geq 10^3) \end{cases} \tag{17}$$

where F_{ig} in Equation (14) included gravity and buoyancy, N; F_{ip} is the pressure, Pa; F_{ib} includes all external forces, N; the formula for calculating the Reynolds number is as follows:

$$\mathrm{Re}_d = \frac{\rho_g |U_{rel}| D_d}{\mu_g} \tag{18}$$

where D_d is the outer diameter of the oil droplet, mm; μ_g is the gas dynamic viscosity, N·s/m^2; and the particle acceleration equation is:

$$\frac{du_{id}}{dt} = \frac{3}{4} C_d \frac{\rho_g}{\rho_d} \frac{1}{D_d} |u_{ig} - u_{id}| (u_{ig} - u_{id}) + \left(1 - \frac{\rho_g}{\rho_d}\right) g_i \tag{19}$$

where u_{id} and u_{ig} are the velocity of the ideal gas and liquid, m/s; g_i is the gravitational acceleration.

(2) Spray sub model

In the simulation process, it is necessary to establish a continuity equation for both the gas and the oil droplet and obtain its numerical solution. The functional form of the spray droplet motion process can be expressed as:

$$\begin{aligned} &\tfrac{\partial f}{\partial t} + \nabla x_i (f \times u_{id}) + \nabla u_{id} (f \times a_i) + \tfrac{\partial}{\partial D_d} (f \times D_d) \\ &+ \tfrac{\partial}{\partial T} \left(f \times \tfrac{dT}{dt}\right) + \tfrac{\partial}{\partial m_d} \left(f \times \tfrac{dm_d}{dt}\right) = \tfrac{d}{dt} f_s \end{aligned} \tag{20}$$

where a_i is the unit mass forces acting on the drop, N; f_s is the droplet generation source term, and its composition is as follows:

$$f_s = f_{inj} + f_{ato} + f_b + f_{col} + f_{imp} + f_T \quad (21)$$

where f_{inj} is the droplet that is injected into the cylinder; f_{ato} is the droplet from the first jet split; f_b is the reaction factors from the second jet split; f_{col} is the effect of the interaction between the droplets during the injection process; f_{imp} is the variation of droplet distribution function; f_T is the influence of irregular turbulence on droplet movement.

(3) Evaporation model

The evaporation of droplets is affected by factors such as heat transfer, convection heat transfer, and heat radiation. The multi-component model was selected to analyze the evaporation process of biodiesel droplets, and the calculation formula was as follows:

$$\frac{dm_d}{dt} = \frac{a_2(T_d - T_0)A}{L} \quad (22)$$

$$m_d C_{pd} \frac{dT_d}{dt} = L(\frac{dm_d}{dt} + \frac{d_{d2}}{dt}) + Q_0 \quad (23)$$

where T_0 is the temperature of each component, K; a_2 is the heat transfer coefficient caused by overheating; m_d is the droplet mass, g; T_d is the temperature of the droplet mass, K; C_{pd} is the droplet specific heat, J/(kg·k); L is the latent heat of evaporation, J/kg; Q_0 is the convective heat transfer between gas and liquid droplets, J.

(4) Wave break up model

In this paper, the WAVE model is selected to simulate the surface breakage of oil droplets. The basic break up time formula is as follows:

$$\tau = \frac{3.7626 \times C_2 \times r}{\lambda\Omega} \quad (24)$$

where Ω is the maximum surface wave generation rate, m/s; λ is the wavelength, m; C_2 is the breaking time, s; r is the droplet radius, mm; and the sub-droplet radius is as follows:

$$r_{stable} = \min\begin{cases} (\frac{3\pi r^2 U_{rel}}{2\Omega})^{0.33} \\ (\frac{3r^2\lambda}{4})^{0.33} \end{cases} \quad (25)$$

where the radius of the mother droplet changes according to the following rules:

$$\frac{dr}{dt} = \frac{-(r - r_{stable})}{\tau} \quad (26)$$

2.2.3. Combustion Model

In general, the combustion process is modeled using two different approaches: General Gas Phase Reactions (GCPR) and combustion model ECFM-3Z+ [32]. In this paper, the combustion process can be modeled using chemical kinetics for biodiesel and ethanol, described with 122 species and 430 reactions employed. To obtain the mass fraction of each chemical species in the gaseous phase, an additional transport equation is solved. The source term in the species transport equation is calculated as:

$$\omega = A{T_r}^B \times e^{-\frac{\beta}{RT}} \quad (27)$$

where A, B, and β are the constants given by the CHEMKIN according to the experimental investigation; T_r is the reaction temperature, °C. If the species is a reactant, it will be calculated as follows:

$$\frac{\partial}{\partial t}(\rho y_k) + \frac{\partial}{\partial k_i}(\rho u_i y_k) = \frac{\partial}{\partial k_i}(\Gamma_k \frac{\partial y_k}{\partial k_i}) + S_k \quad (28)$$

where y_k represents the mass fraction of an individual chemical species k, g; S_k is the species source term, and considering the difference between forward and backward reactions, the concentration of chemical species in these reactions can be calculated as follows:

$$S_k = \frac{dc_i}{dt} \times M_i = \sum_{n=1}^{f} (\omega_{n,f} \times c_{nf} \times c_{oxy}) - \sum_{n=1}^{b} (\omega_{n,b} \times c_{n,b} \times c_{red}) \tag{29}$$

where f is the number of forwarding chemical reactions; b is the number of backward chemical reactions; c_{oxy} and c_{red} are the molar concentrations of the oxidizer and redactor, respectively, mol/L; $c_{n,f}$, and $c_{n,b}$ represent molar concentrations of all species that participate in forwarding chemical reactions, mol/L.

2.2.4. Emission Model

In the combustion process, the Extended Zeldovich model is employed to simulate the NO_x emission due to the mechanism mainly considering the real diesel engine working condition [33]. In addition, the equations that control the soot generation in the AVL-Fire are as follows:

$$S_{ps} = S_t + S_u + S_{oxy} \tag{30}$$

where S_{ps}, S_t, S_u, and S_{oxy} are the soot source item, nucleus source item, soot surface generation source item, and soot oxidation source item, respectively, kg/m^3-s; and the nucleation source item can be expressed as:

$$S_t = C_t \exp\left\{ \frac{-(f - f_t)^2}{\sigma_t^2} \right\} \tag{31}$$

where C_t is the maximum nucleation rate, m^3/s; f is the fuel mass fraction; f_t is the maximum nuclei mass fraction; σ_t is the variable of f_t.

The soot surface generation source item is as follows:

$$S_u = C \times F(f, \varphi_t) \times p^{0.5} \times e\left\{ -\frac{E_a}{RT} \right\} \tag{32}$$

where E_a is the activation energy, kJ/mol; R is the real gas constant; p is the pressure, pa; T is the temperature, °C; F (f, φ_t) is the surface generation rate function; f is the mixture mass fraction; φ_t is the soot mass fraction.

The soot oxidation can be expressed as:

$$S_{oxy} = -F(\varphi_t, P_{oxy}, T) \tag{33}$$

$$S_{oxy} = -F(\varphi_t, P_{oxy}, \tau) \tag{34}$$

where τ is the integral turbulent time scale, P_{oxy} is the function of the pollution generation rate.

2.3. Ethanol and Biodiesel Mechanism

In this study, an improved skeletal reaction model was constructed by combining two skeletal reaction mechanisms of biodiesel and ethanol. It was employed to simulate the blend fuel oxidation and emission formation processes. The former kinetic model for biodiesel was a three-component developed by Luo et al. [34] which was composed of methyl decanoate (MD), methyl-9-decanoate (MD9D), and n-heptane. Usually, MD was used to represent the saturated FAMEs, while MD9D was used to represent the unsaturated FAMEs, and n-heptane was used to match the input energy and the C/H/O ratio. It consists of 115 species and 460 reactions. The 1 mol biodiesel was assumed to be composed of 0.25 mol MD, 0.25 mol MD9D, and 0.5 mol of n-heptane. The later reduced kinetics mechanism was developed from the detailed oxidation framework of ethanol proposed by

Li et al. [35], and it was widely used as the base mechanism for the multi-component fuel chemistry formulation process.

2.4. 3D-CFD Model and Computational Mesh

In the present paper, a diesel engine cylinder combustion chamber was built using AVL-Fire software. Table 1 shows the main parameters of the diesel engine. Due to the geometry of the diesel engine, the combustion chamber, and nozzle are axisymmetrically distributed, a one-sixth combustion chamber and nozzle model was selected to analyze the combustion and emission characteristics of the diesel engine. The computation model is shown in Figure 2.

Table 1. Key parameters for the diesel engine.

Performance Index	Unit	Value or Description
Engine type	-	Four-cylinder, turbocharged,
Bore × stroke	mm	93 × 102
Number of cylinders	-	4
Engine speed	rpm	1800
Rating power output	kW	72
Nozzle orifice diameter	mm	0.23
Fuel injection holes	-	6
Connecting rod	mm	168
Compression ratio	-	18

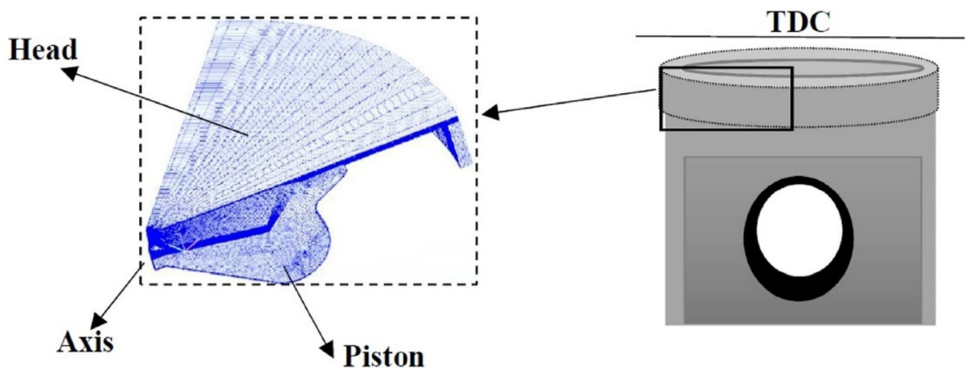

Figure 2. Piston scheme and designed grid of a part piston bowl at TDC position [36].

Furthermore, to predict accurately the cylinder inflow and combustion process, three different refinement cylinder chambers at Top Death Center were employed and known as coarse, medium, and fine girds. Figure 3a–c shows the basic structure of the three different grids and the numbers of the three girds are 71,572, 160,764, and 310,408. Figure 4 shows the cylinder pressure curves of the three different girds for fossil diesel at full load. The result indicates that there is no significant difference between fine gird and medium gird. Therefore, medium gird was selected in this study.

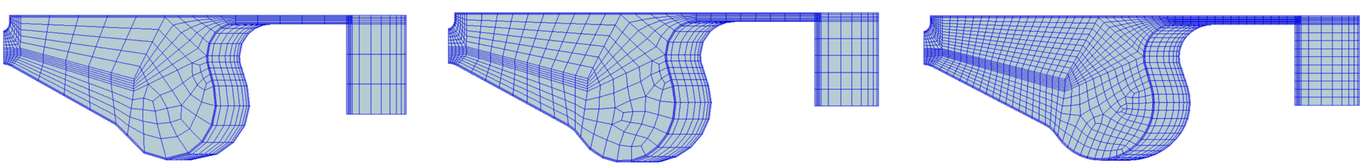

(**a**) (**b**) (**c**)

Figure 3. Three calculation girds: (**a**) coarse girds, (**b**) medium girds, and (**c**) fine girds.

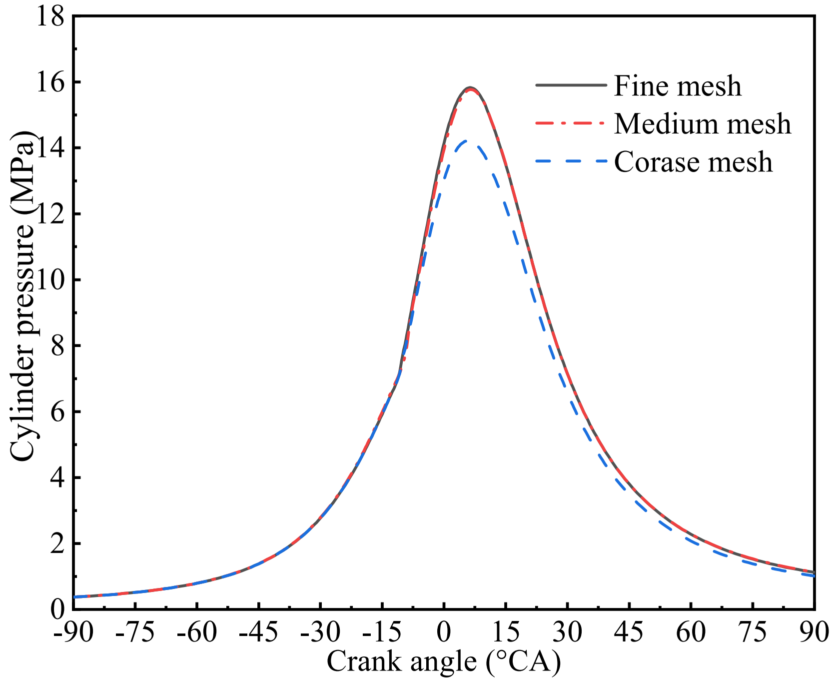

Figure 4. The cylinder pressure comparison of grid independence test.

2.5. Fuel Blend Rates and Properties

In this paper, the test biodiesel produced from soybean crude oil was prepared by a method of alkaline catalyzed transesterification. 200 mL CH_3OH plus the required amount of KOH was added for every liter of soybean crude oil, and the reactions were carried out at 45 °C. The water wash process was performed using a sprinkler, which slowly sprinkled water into the biodiesel container until there was an equal amount of water and biodiesel in the container. The water/biodiesel mixture was then agitated gently for 10 min, allowing the water to settle out of the biodiesel. After the mixture had settled, the water was drained out [37]. Table 2 shows the fatty acid compositions of the biodiesel.

Table 2. Physical properties of FAMEs in soybean biodiesel.

Type	Kinetic Viscosity (mm^2/s) (at 40 °C)	Density (g/cm^3) (at 20 °C)	Molecular Weight (g/mol)	Higher Calorific Value (MJ/kg)	SME (%)
C18:3	3.11	0.899	292	39.43	6.19
C18:2	3.79	0.887	294	39.68	55.19
C18:1	4.60	0.875	296	39.93	23.43
C18:0	5.59	0.863	298	40.18	3.22
C16:0	4.37	0.864	270	39.56	11.98

In the paper, the ethanol is blended with biodiesel due to the good mutual solubility. BE5 represents 95% biodiesel and 5% ethanol by vol.; BE10 represents 90% biodiesel and 10% ethanol by vol.; BE15 represents 85% biodiesel and 15% ethanol by vol.; BE20 represents 80% biodiesel and 20% ethanol by vol.; B100 represents pure biodiesel without ethanol addition and D100 represents pure biodiesel without ethanol addition. Table 3 shows the chemical and physical properties of diesel, biodiesel, and ethanol.

Table 3. Properties of the test fuel.

Property	Diesel	Biodiesel	Ethanol	BE5	BE10	BE15	BE20
Cetane number	50	53	6	-	-	-	-
Lower heating value (MJ/kg)	42.5	37.5	28.4	37.1	36.7	36.2	35.7
Density (kg/m^3) @ 20 °C	840	871	786	867	862	858	854
Viscosity (mm^2/s) @ 40 °C	2.86	5.28	1.2	-	-	-	-
Heat of evaporation (kJ/kg)	250–290	300	840	324.5	349.2	374.2	408
Carbon content (% mass)	86.6	77.1	52.2	76.0	74.8	73.7	72.1
Hydrogen content (% mass)	13.4	12.1	13	12.1	12.2	12.2	12.3
Oxygen content (% mass)	0	10.8	34.8	11.9	13.0	14.1	15.6
Sulfur content (mg/kg)	10	10	0	-	-	-	-

2.6. Feasibility Test

In this paper, in order to validate the model, the experiment should be carried out. Figure 5 shows the schematic diagram of diesel engine test equipment. The TCHK-400U was used to measure the exhaust gas temperature. The BILSA MOD 210 infrared gas analyzer was used to measure the gas emission. The AVL-Smoke meter was used to measure the soot emission. The FCMM-2 was used to measure fuel mass. The DEWE-2010CA combustion analyzer was used to monitor the combustion of the diesel engine. The EFS-IFR600 was used to measure fuel injection rate with a measurement error of 0.5%. A hydraulic dynamometer was used to measure diesel engine load. In addition, an Electronic Control system was employed for controlling the electronically controlled diesel engine. Table 3 indicates the measurement range of each test instrument and its permissible error range.

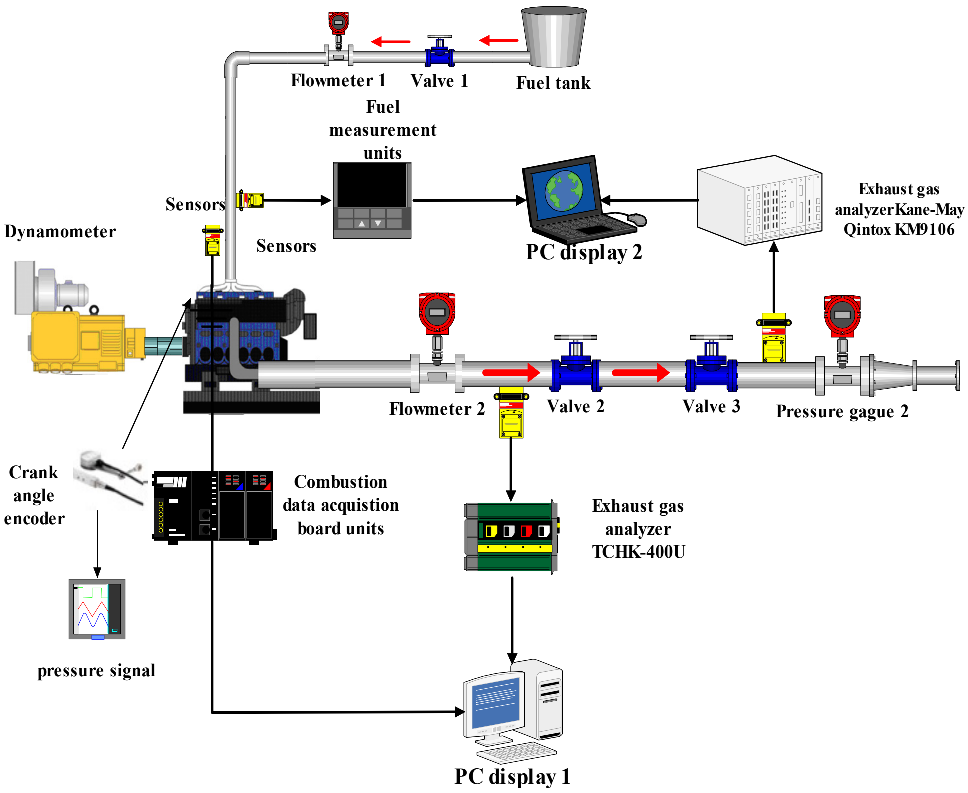

Figure 5. The schematic diagram of the experimental device.

2.7. Uncertainty Analysis

In general, the experimental measurements obtained have some uncertainties and errors. Table 4 shows the list of measurements, measuring accuracy, and measuring range. The uncertainty in the experimental results will arise from the condition, calibration, sensor selection, test procedure, and observation [38]. In this study, the uncertainty of the calculation parameters was given by Equation (34). The R_b in Equation (35) is a function of the independent variables K_1, K_2, ..., and K_n. The t_1, t_2, ..., and t_n are the independent variable uncertainties, respectively.

$$E_R = \left\{ [(\partial R_b/\partial K_1)t_1]^2 + [(\partial R_b/\partial K_2)t_2]^2 + \cdots [(\partial R_b/\partial K_n)t_n]^2 \right\}^{1/2} \quad (35)$$

$$R_b = \{K_1,\ \mathrm{K}_2,\ \mathrm{K}_3,\ \cdots K_n\} \quad (36)$$

Table 4. List of measurements, measuring accuracy, and measuring range.

Measurements	Measuring Range	Accuracy	Uncertainty (%)
Cylinder pressure	0–25 MPa	±10 kPa	±0.5
Exhaust gas temperature	0–1000 °C	±1 °C	±0.25
Brake power	-	±0.03 kW	±0.03
Air flow mass	0–33.3 kg/min	±1%	±0.5
Engine speed	1–2000 rpm	±10 rpm	±0.24
Fuel flow measurement	0.5–100 L/h	±0.04 L/h	±0.5
CO emission	0–16%vol	±0.03%	±0.32
Soot emission	0–9 FSN	±0.1 FSN	±2.8
NO_x emission	0–5000 ppm	±10 ppm	±0.56
BSFC	-	±5 g/kW·h	±1.5
Crank angle encoder	0–720 °CA	±0.2 °CA	±0.3

In this paper, the total uncertainty in the experimental study produced can be calculated from the following equation.

Total experimental uncertainty = Square root of [(uncertainty of cylinder pressure)^2 + (uncertainty of exhaust gas temperature)^2 + (uncertainty of brake power)^2 + (uncertainty of air flow mass)^2 + (uncertainty of CO emission)^2 + (uncertainty of Soot emission)^2 + (uncertainty of NO_x emission)^2 + (uncertainty of BSFC)^2 + (uncertainty of crank angle encoder)^2] = Square root of [$(0.5)^2 + (0.25)^2 + (0.03)^2 + (0.5)^2 + (0.32)^2 + (2.8)^2 + (0.56)^2 + (1.5)^2 + (0.3)^2$] = 3.340%

2.8. Model Validation

In this paper, in order to accurately simulate the combustion and emission characteristics of biodiesel with different ethanol addition ratios. An improved mechanism including three-component biodiesel mechanism and ethanol combustion mechanism was used to investigate the effects of ethanol addition ratios on performance, combustion, and emission characteristics. The comparisons of the experiment and simulation at different loads are shown in Figures 6 and 7. It can be found that the simulation results agree better with the experiment results. Thus, the simulation computational modeling can be employed to predict the blended fuel combustion process.

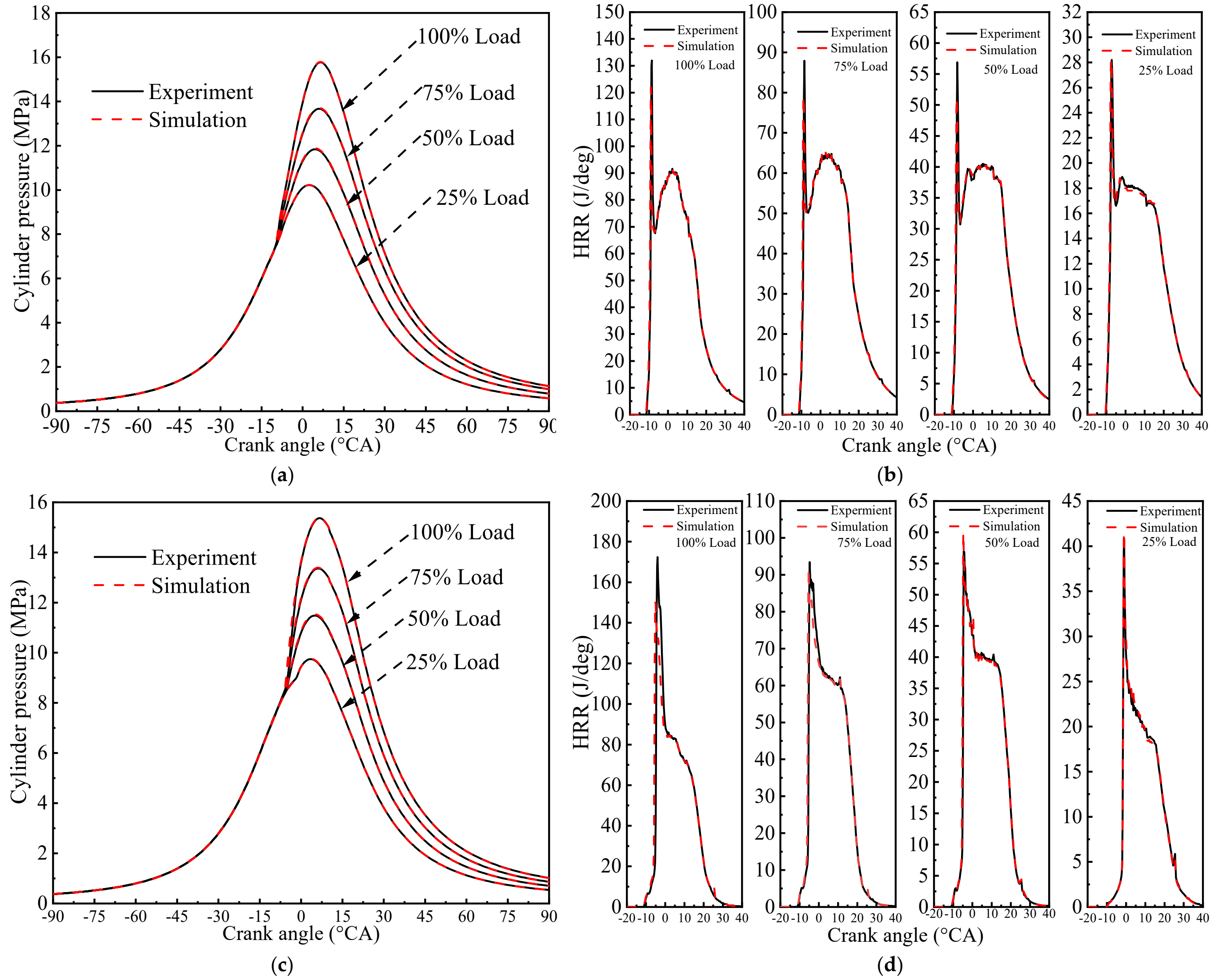

Figure 6. Comparison of cylinder pressure (**a**,**c**) and HRR (**b**,**d**) of D100 and BE10. (**a**) D100 Cylinder pressure. (**b**) D100 Heat release rate. (**c**) BE10 Cylinder pressure (**d**) BE10 Heat release rate.

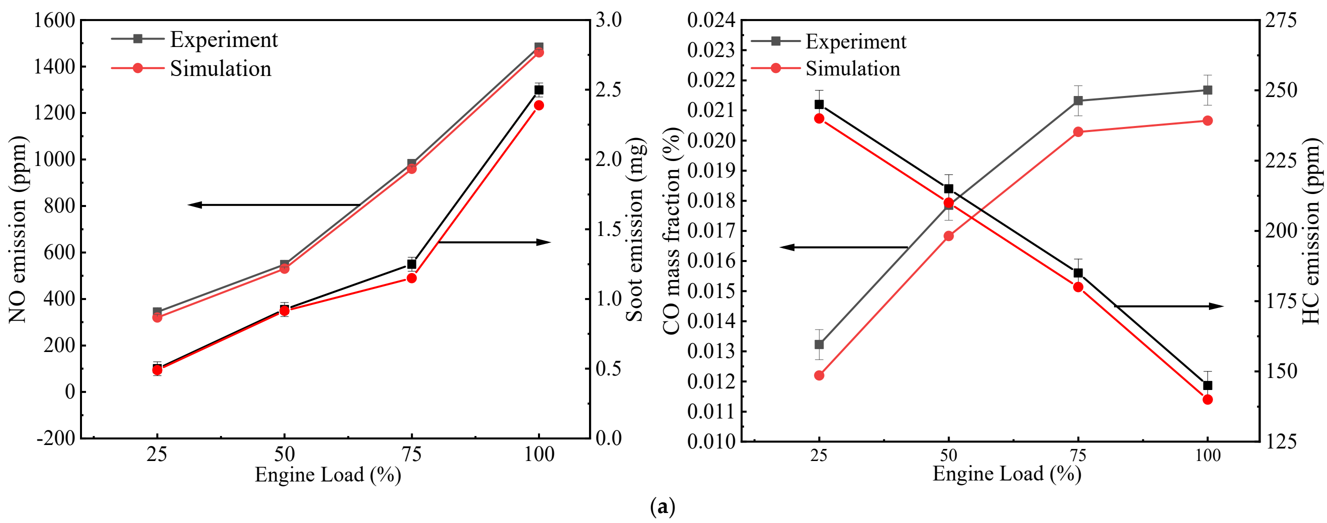

Figure 7. *Cont.*

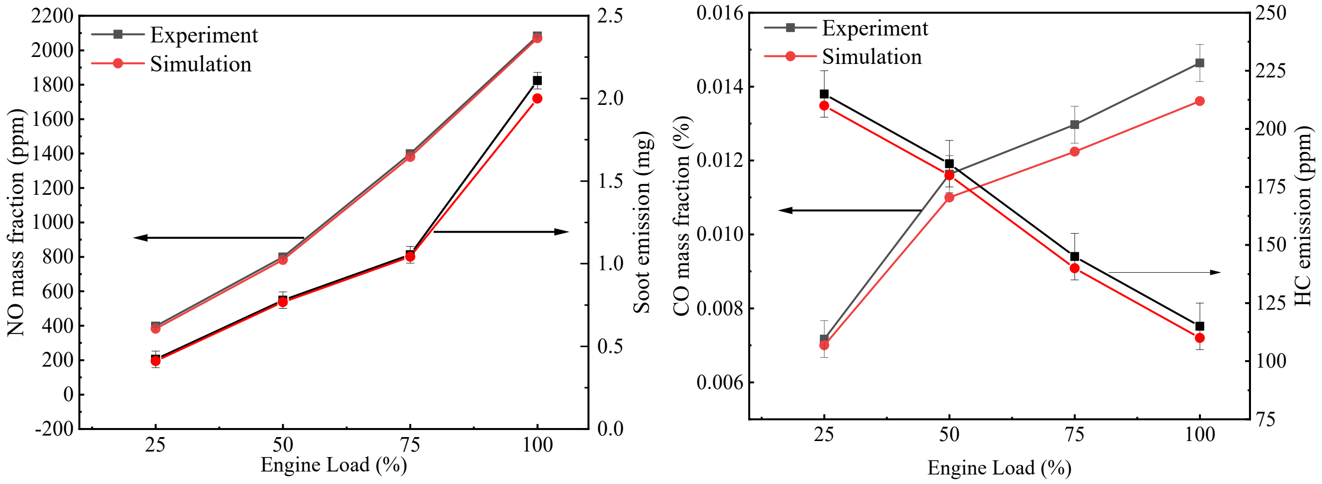

(**b**)

Figure 7. Comparisons of emissions (CO, Soot, HC, and NO_x) of (**a**) D100 and (**b**) BE10. (**a**) D100 emissions validation. (**b**) BE10 emissions validation.

3. Results and Discussion

In this paper, the different biodiesel-ethanol-blended fuels were employed to study the combustion and emission characteristics of diesel engines at different loads. The main focus is on the effect of ethanol added to biodiesel on engine power, brake specific fuel consumption, brake thermal efficiency, carbon monoxide emission, soot emission, and nitrogen oxide emission.

3.1. Engine Performance

3.1.1. Brake Power

Figure 8 indicates the brake power for different fuels at different loads. It can be seen that the diesel indicates the highest brake power at all loads. However, pure biodiesel and biodiesel/ethanol-blended fuel have worse performance in all cases. Specifically, the brake power of biodiesel decreases by 11.63% at full engine load. This is due to the lower heating value. In addition, the result also indicates that with the increase in ethanol addition ratios, the brake power of the blended fuel is decreased. For instance, compared with diesel at full engine load, the brake powers of BE5, BE10, BE15, and BE20 blended fuels are decreased by 13.71%, 14.23%, 15.54%, and 16.85%, respectively. This is mainly attributed to the lower heating value of ethanol. A similar trend was also observed by Shirneshan [38] due to the reduction in the heating value of the blends containing ethanol.

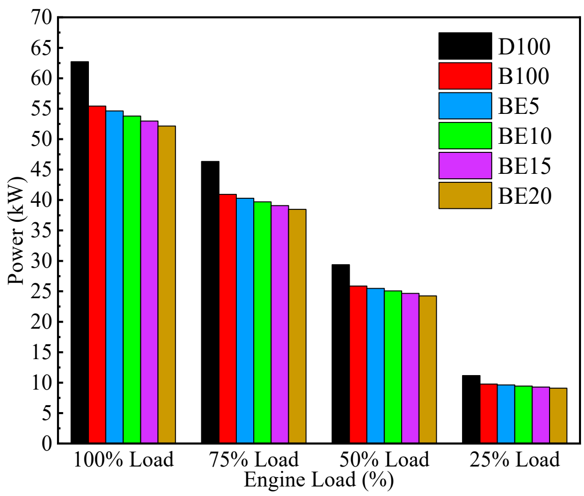

Figure 8. Comparisons of brake power for different fuels at different loads.

3.1.2. Brake Specific Fuel Consumption

BSFC shows that an engine transforms the provided energy into the beneficial work output [39]. Figure 9 indicates the BSFC for different fuels at different loads. It can be seen that the BSFCs of the blended fuels increase with increase in ethanol addition ratios. Specifically, the BSFCs of BE5, BE10, BE15, and BE20 are increased 12.46%, 13.42%, 15.44%, and 18.64%, respectively, at full engine load. The increased BSFC for the blended fuel is mainly due to the lower heating value and higher density of biodiesel. More specifically, the lower heating value of the biodiesel is lower about 11.76% and the density of the biodiesel is higher about 3.69%. Therefore, with the increase in ethanol addition ratios, a higher volume of fuel was injected into the cylinder to compensate for the lower heating value of biodiesel and ethanol [40].

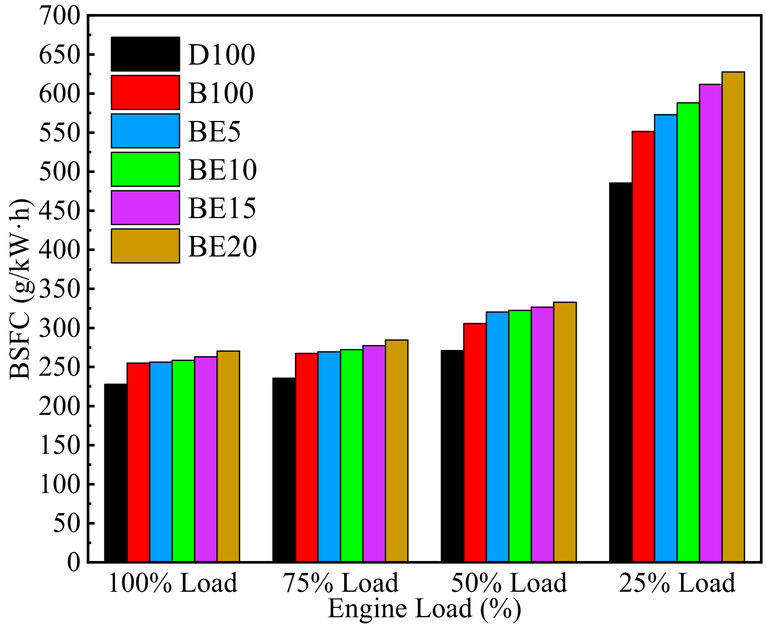

Figure 9. Comparison of BSFC for different fuels at different loads.

3.1.3. Brake Thermal Efficiency

The BTE is the brake power produced by the engine to the energy released per unit of time when the fuel is complete combustion and is an important indicator to measure the work capacity of the engine [41]. The BTE can be calculated by the following formula:

$$BTE = \frac{3600}{BSFC \times LHV} \tag{37}$$

where LHV is the fuel's low heating value, MJ/kg.

Figure 10 indicates the BTE values for different fuels at different loads. It can be seen that the engine loads have a significant effect on the BTE of blended fuels. At low load, the BTE of the blended fuels and biodiesel were lower compared with diesel. This is because the lower heating value and lower cetane number of ethanol further decreased the combustion temperature and increased the ignition delay, which should be responsible for the lower BTE of the blended fuels at a low load. With the increase in engine load, the BTEs of the blended fuels gradually increase. Specifically, the BTEs of B100, BE5, BE10, BE15, and BE20 are increased 1.32%, 1.86%, 2.09%, 1.70%, and 1.33% respectively, at full engine load. The reason for this consists of two aspects. First, the lower heating value of ethanol and the larger latent heat of vaporization result in a lower cylinder temperature decreases with engine load increases. Second, the oxygen content of the blended fuels can increase the combustion efficiency in the cylinder, which leads to the increase in BTE for the blended fuels at full engine load [42].

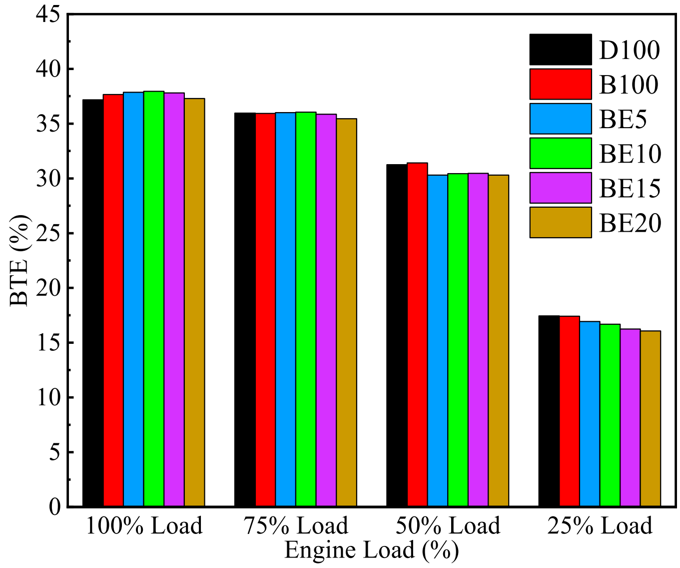

Figure 10. Comparison of BTE for different fuels at different loads.

3.2. Combustion Characteristics

3.2.1. Cylinder Pressure

Figure 11a–d indicates the in-cylinder pressure curve for different fuels at different loads. It can be seen that pure diesel indicates the highest in-cylinder pressure at all engine loads, followed by B100, BE5, BE10, BE15, and BE20. Specifically, compared with diesel, the maximum cylinder pressure values of B100, BE5, BE10, BE15, and BE20 are decreased by 1.51%, 1.96%, 2.53%, 3.01%, and 4.31% respectively, at full engine load. The decrease in in-cylinder pressure could be attributed to the ethanol's lower heating value and cetane number. More specifically, the increased ethanol addition ratios reduce the cetane number of the blended fuels compared with diesel. Meanwhile, the high heat vaporization of ethanol also decreases the working temperature in the cylinder. Thus, the blended fuels indicate lower cylinder pressure compared with diesel. A similar trend was also found by Zuo et al. [43] and Tongroon et al. [44]. Therefore, the high latent heat of vaporization of ethanol leads to an increase in ignition delay and a decrease in the heat release rate.

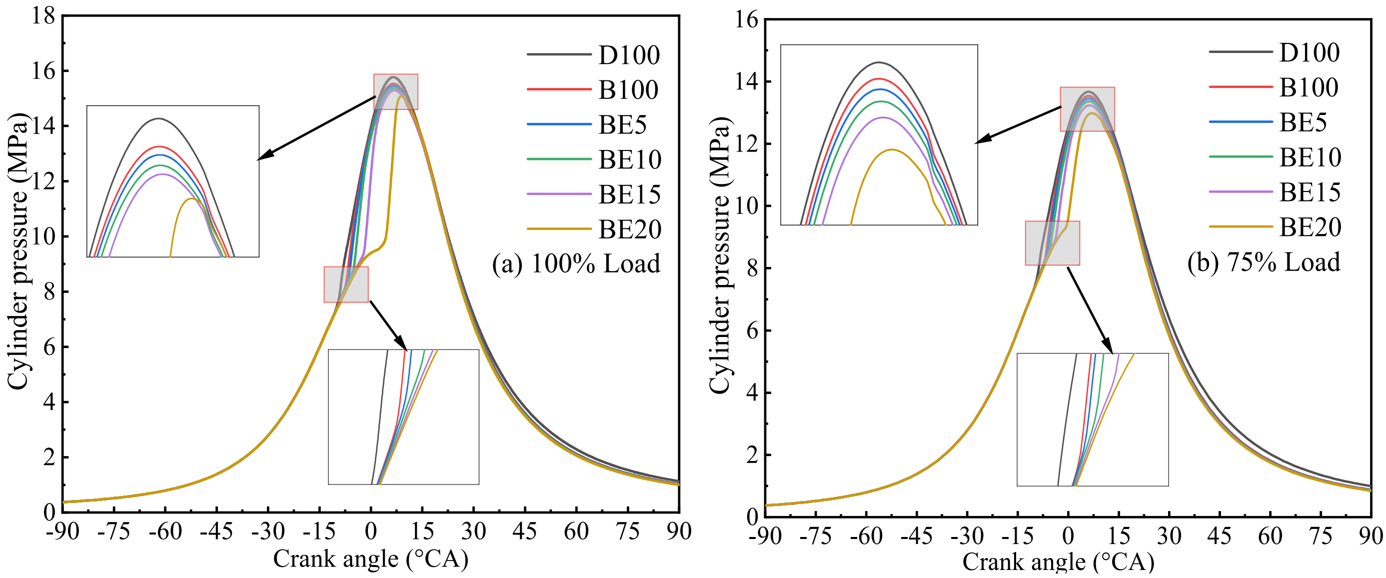

Figure 11. *Cont.*

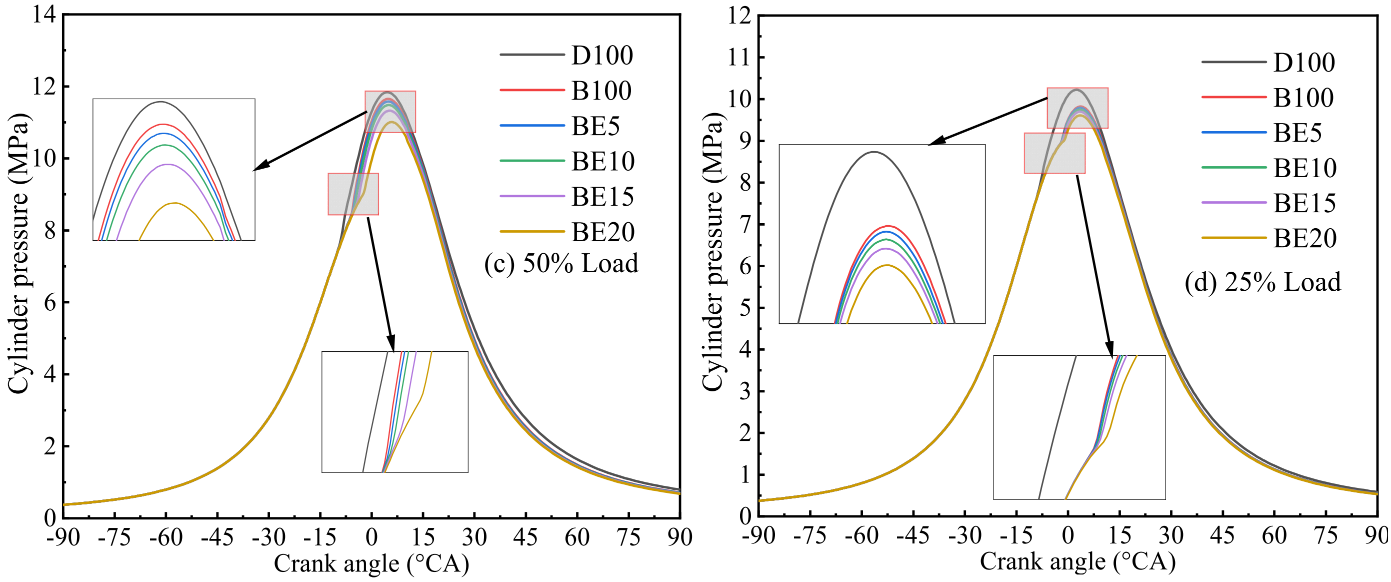

Figure 11. Comparison of cylinder pressure for different fuels at different loads. (**a**) 100% Load, (**b**) 75% Load, (**c**) 50% Load, (**d**) 25% Load.

3.2.2. Cylinder Temperature

Figure 12a–d indicates the in-cylinder temperature curves for different fuels at different loads. It can be seen that the in-cylinder temperature decreases significantly with the increase in ethanol ratios. Specifically, compared with diesel, the maximum cylinder temperature values of B100, BE5, BE10, BE15, and BE20 are decreased 0.136%, 0.549%, 0.948%, 1.23%, and 0.628%, respectively, at full engine load. It is due to the lower cetane number and heating value of ethanol. Lower cetane number of ethanol increased the ignition delay. Thus, the different ethanol addition ratios significantly affect the in-cylinder temperature curves. In addition, the high vaporization of ethanol results in more heat loss, especially at low load.

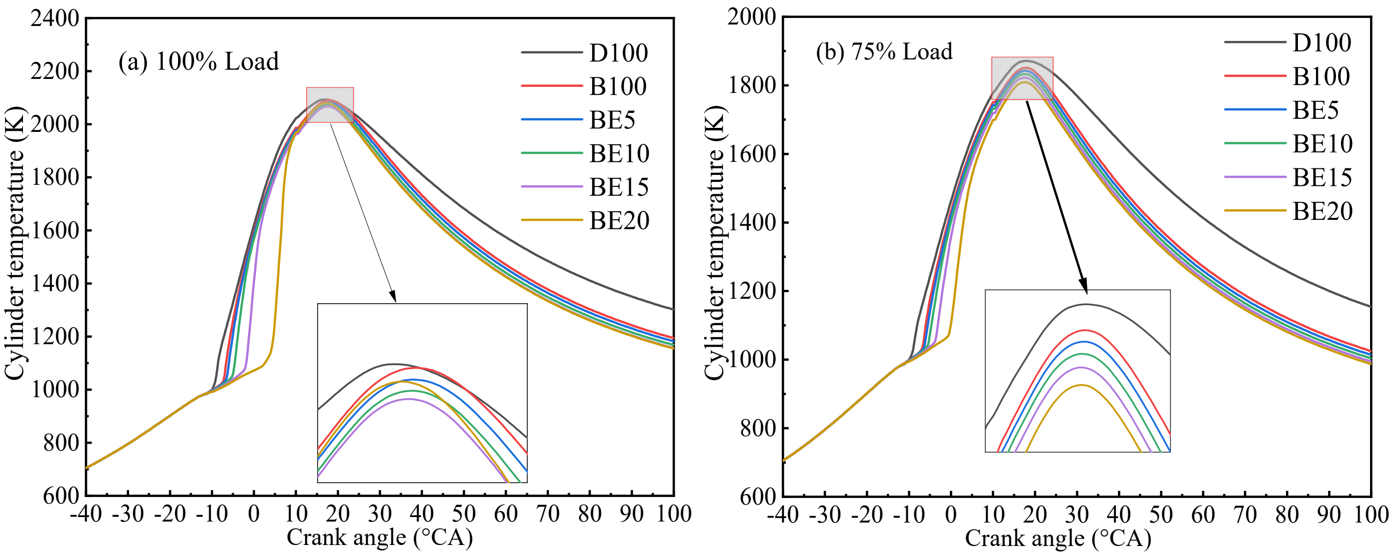

Figure 12. *Cont.*

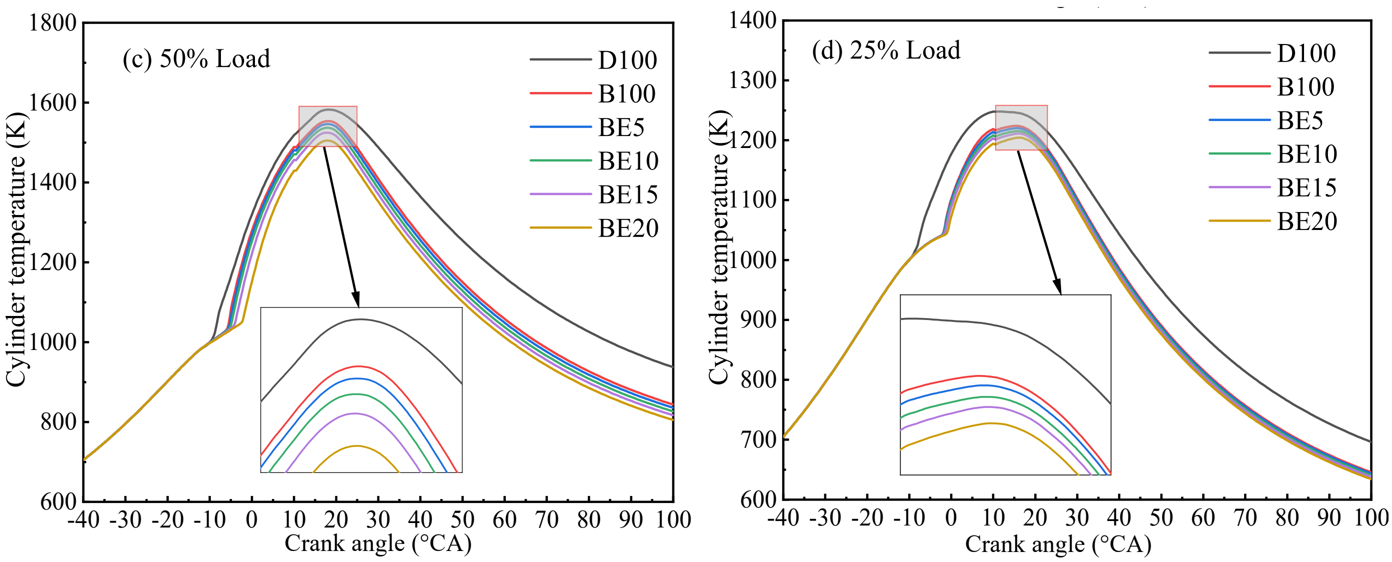

Figure 12. Comparison of cylinder temperature for different blends at different loads. (**a**) 100% Load, (**b**) 75% Load, (**c**) 50% Load, (**d**) 25% Load.

Table 5 indicates the in-cylinder temperature distribution field of different fuels at full engine load. It can be seen that the ethanol addition decreases the localized higher temperature zones due to higher latent heat vaporization of ethanol. Moreover, the oxygen content in biodiesel also has a positive effect on improving the combustion characteristics of the blend fuel. With the increase of ethanol addition ratios, the lower latent heat of vaporization of ethanol results in more heat loss. Therefore, the ethanol addition decreases the cylinder temperature.

Table 5. Cylinder temperature distribution field in the cylinder at 100% load.

	−8 °CA	**0 °CA**	**8 °CA**
D100	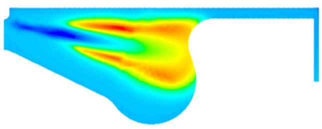	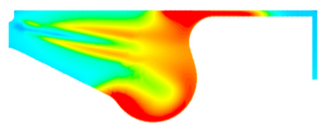	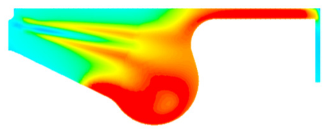
B100		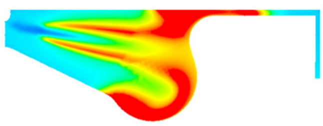	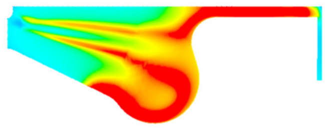
BE5	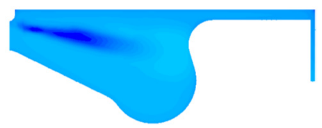	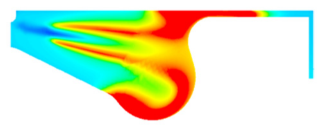	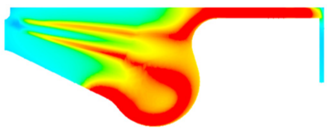
BE10	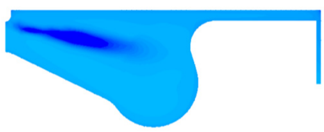	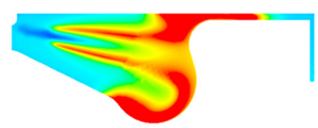	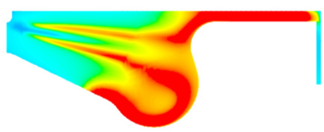
BE15	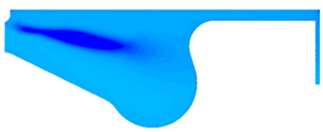	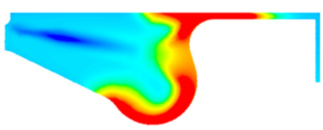	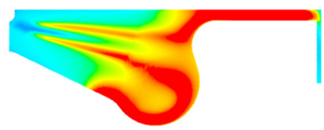

Table 5. *Cont.*

	−8 °CA	0 °CA	8 °CA
BE20	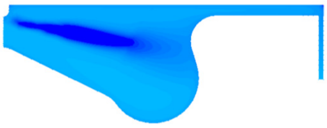	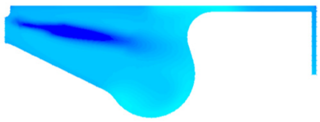	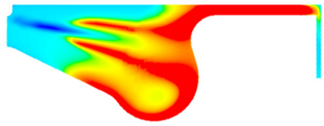

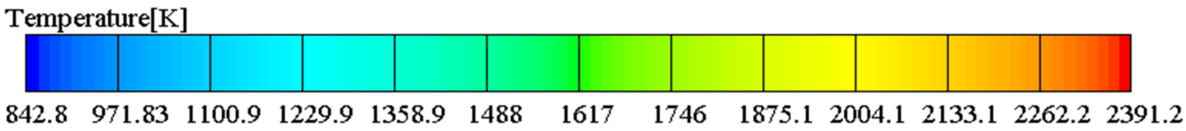

3.2.3. Heat Release Rate

Figure 13a–d indicates the HRRs of different fuels at different loads. It can be seen that with the increase in ethanol addition ratios, the ignition delay of the blended fuels will increase compare with diesel. The ethanol addition ratios played an important role. As seen in Table 5, with the increase in ethanol addition ratios, the HRRs increased. It is due to longer ignition delay caused by the increased ethanol. More specifically, due to the high latent heat of ethanol, the gasification of ethanol extends flame retardation, and lots of unburned homogeneous mixture gases are stored during the premixed combustion phase [45]. Therefore, higher HRRs are indicated with an increase in ethanol. In addition, the higher oxygen content in the blended fuels and biodiesel improves the combustion efficiency [46].

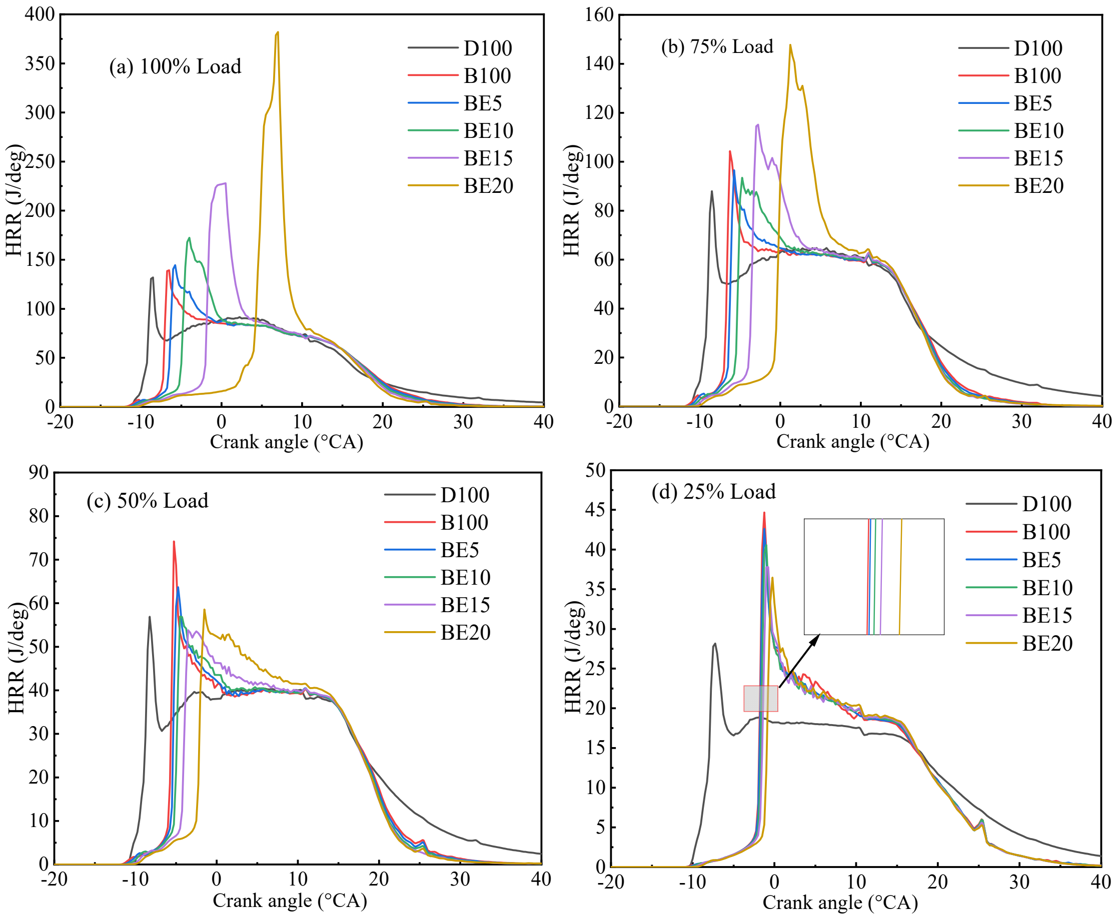

Figure 13. Comparison of HRR curves for different blends at different loads. (**a**) 100% Load, (**b**) 75% Load, (**c**) 50% Load, (**d**) 25% Load.

3.3. Emission Characteristics

3.3.1. Nitrogen Oxide Emission

The in-cylinder temperatures primarily influence the rate of NO_x formation according to the well-accepted Zeldovich mechanism [44]. Figure 14a–d indicates the NO_x emission of different fuels at different loads. At low load, the NO_x mass fraction is higher than for biodiesel as compared to fossil diesel. It is due to the local high temperature area caused by the high viscosity. In addition, it can be seen that with the increase of engine loads, the NO_x emission increases. This is due to the high in-cylinder temperatures caused by the increased fuel mass injected into the cylinder. Furthermore, pure biodiesel indicates more NO_x emission compared with diesel. This is due to the improved combustion caused by the higher oxygen content [47,48]. In addition, the ethanol addition ratios also played an important role in NO_x emission. Table 6 indicates the NO_x mass fraction distribution field at 100% load. It can be seen that NO_x mass fraction distribution field decreases with the increase of ethanol ratios. This is because the ethanol addition decreases the in-cylinder temperature. Moreover, the ignition delay is increased by the lower heating value and higher latent heat of ethanol vaporization. Thus, NO_x emission is reduced.

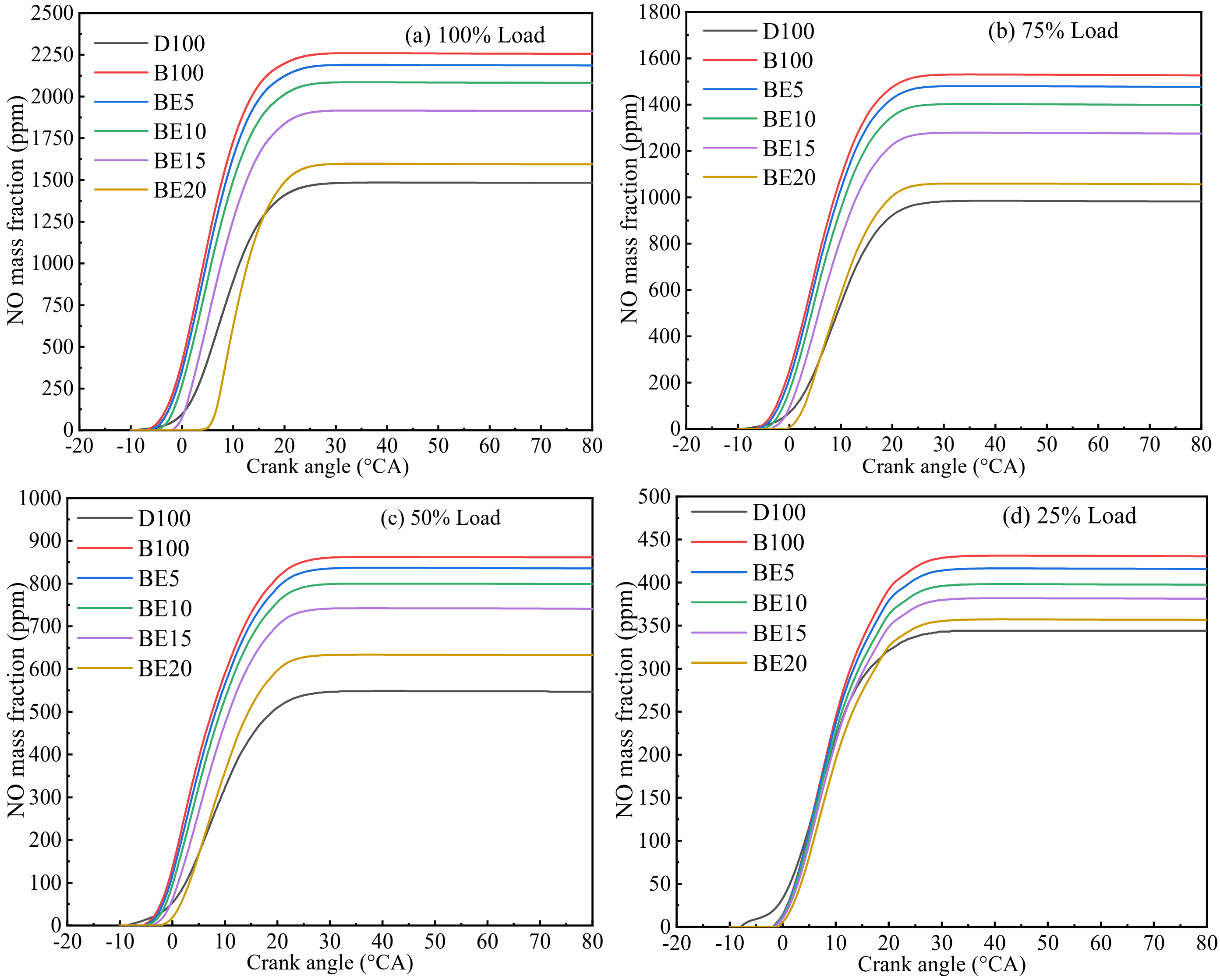

Figure 14. Comparison of NO_x emission for different blended fuels at different loads. (**a**) 100% Load, (**b**) 75% Load, (**c**) 50% Load, (**d**) 25% Load.

Table 6. NO_x mass fraction distribution field in the cylinder at 100% load.

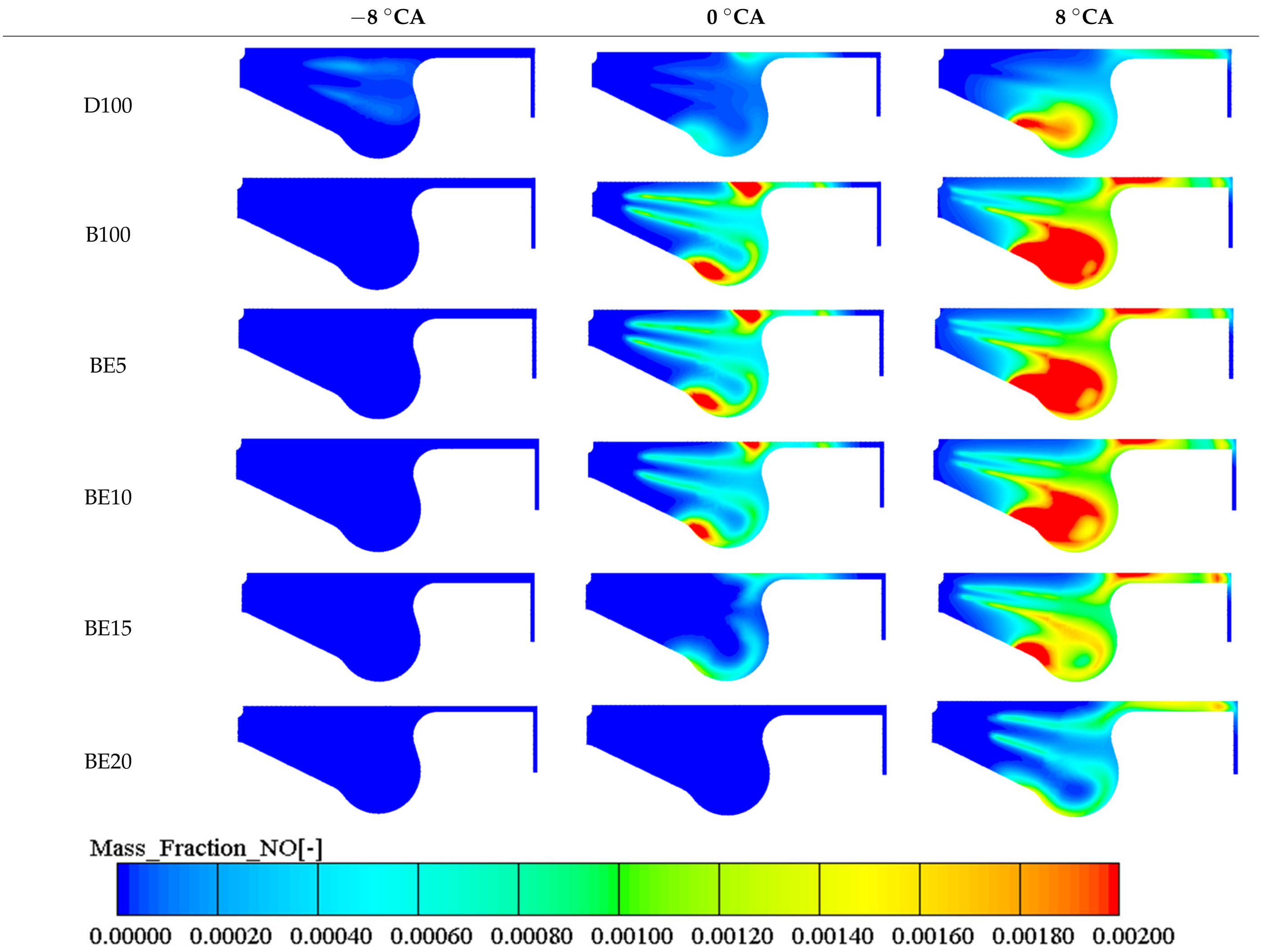

3.3.2. Carbon Monoxide Emission

Figure 15 indicates the CO emission of different fuels at different loads. It can be seen that with the increase of engine loads, the CO emission increases. This is due to the incomplete combustion and low temperature [49]. Specifically, compared with diesel, the CO emissions of B100, BE5, BE10, BE15, and BE20 are decreased by 26.19%, 29.25%, 32.47%, 34.88%, and 39.57%, respectively, at full engine load. This is due to the improved combustion caused by the oxygen in the biodiesel and ethanol. A similar trend was also observed by Sathish et al. [48]. They explained that the ethanol addition ratios led to a decrease in the CO emission in the blended fuels due to their volatility. More specifically, the latent heat of evaporation also leads to a significant contribution to the CO emission decrease.

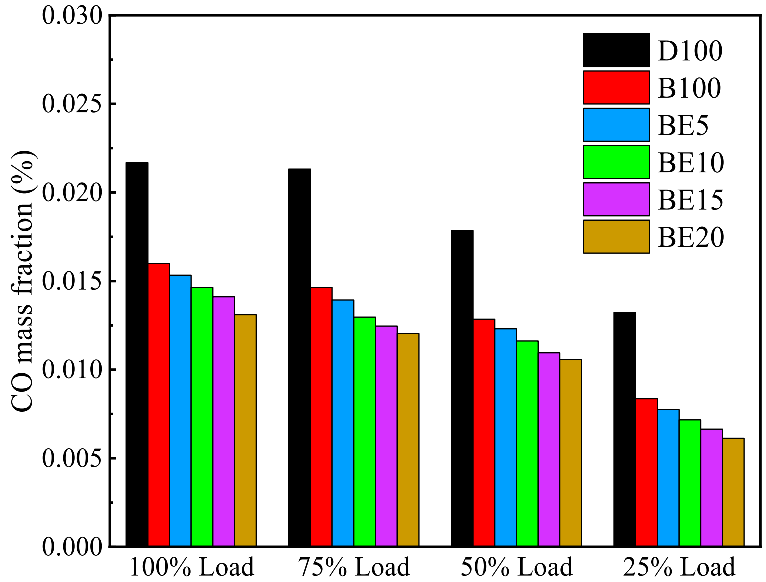

Figure 15. Comparison of CO emission for different blended fuels at different loads.

3.3.3. Soot Emission

Figure 16a–d indicates soot emission for the different fuels at different loads. It can be found that with the increase in engine loads, more soot emission was observed both in pure diesel and blended fuels. When the engine load increases, more fuel is injected into the cylinder. The air-fuel ratio is reduced [50]. Therefore, more soot could be formed in the period of diffusion combustion [51]. In addition, biodiesel has lower soot emission compared with diesel at all loads. This is due to the improved combustion caused by the biodiesel's extra oxygen content. When the diesel engine is fueled with blended fuels, ethanol addition can significantly decrease soot emission. Specifically, compared with diesel, the soot emissions of B100, BE5, BE10, BE15, and BE20 are decreased by 12.19%, 13.25%, 14.5%, 15.64%, and 15.95%, respectively, at full engine load.

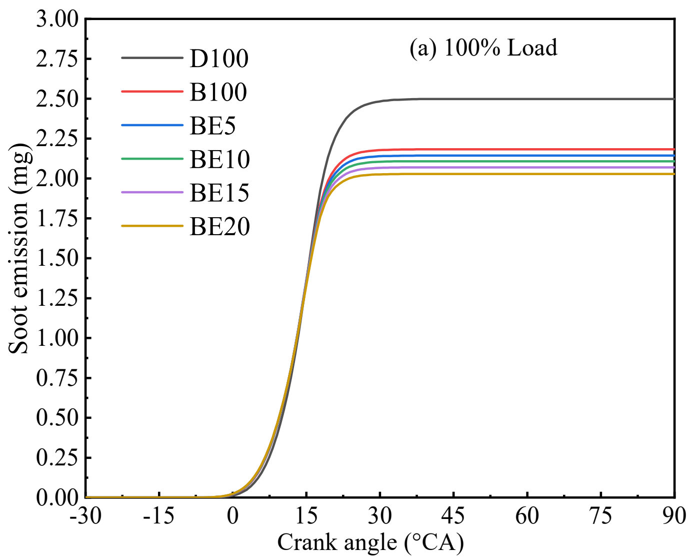

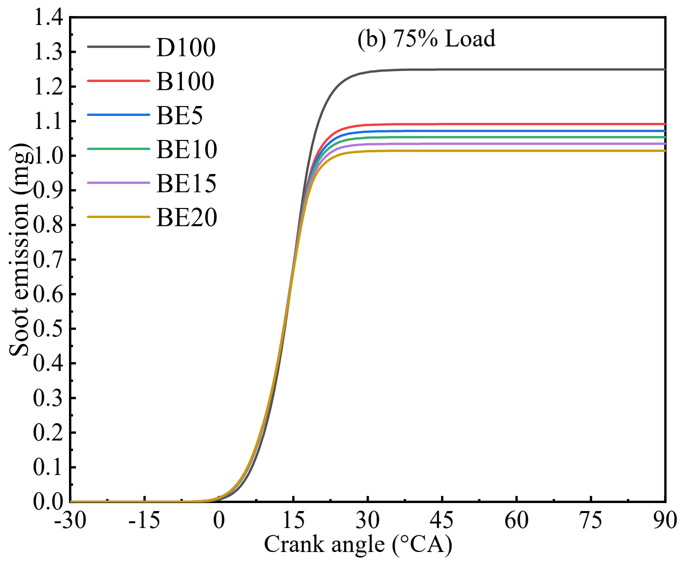

Figure 16. *Cont.*

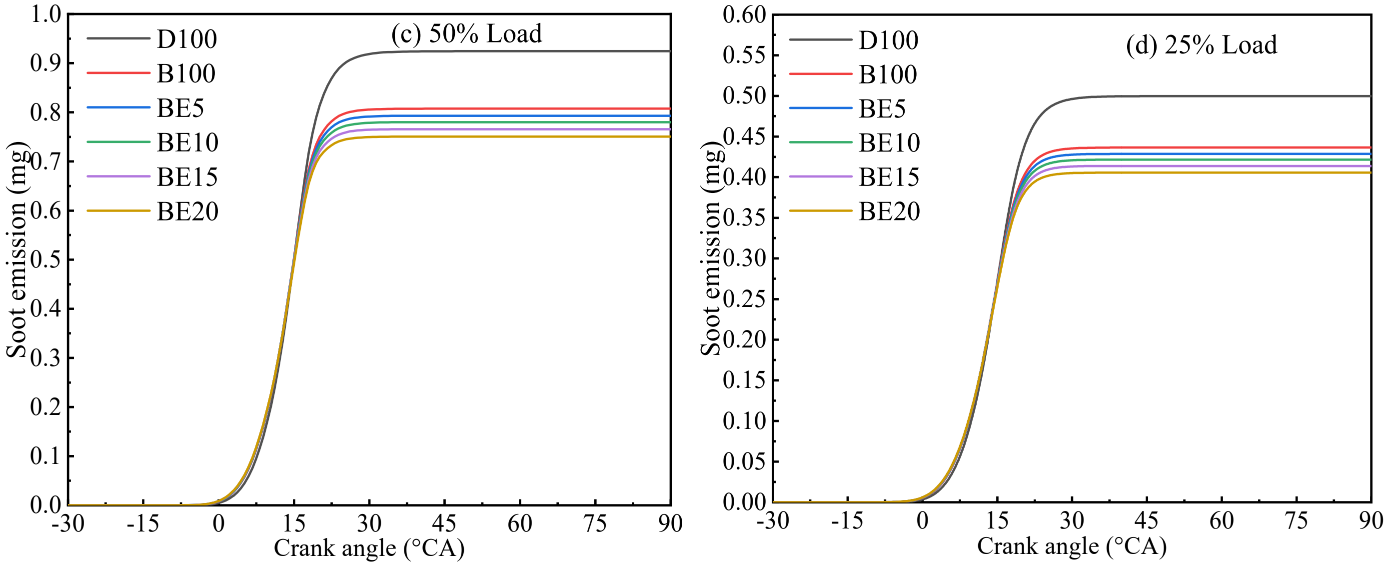

Figure 16. Comparison of soot emission for different blended fuels at different loads. (**a**) 100% Load, (**b**) 75% Load, (**c**) 50% Load, (**d**) 25% Load.

4. Conclusions

With the increasing shortage of energy and the continuous deterioration of the environment, it is urgent to find renewable, carbon-neutral green energy [52–54]. In this paper, a CFD model was established and validated by experiment results. An improved CHEMKIN code including 122 species and 430 reactions was employed to simulate the combustion process. Then, the validated model was used to investigate the effect of different ethanol addition ratios on the combustion, performance, and emission characteristics of diesel engines. The main conclusions obtained are as follows:

(1) Ethanol addition ratios mainly influence the performance characteristic of the diesel engine at different loads. The engine's brake power is reduced and the BSFC is increased due to the lower heating value of ethanol. However, the BTE value of the engine increases with the proportion of ethanol in the blended fuel. More specifically, the BTEs of B100, BE5, BE10, BE15, and BE20 increased by 1.32%, 1.86%, 2.09%, 1.70%, and 1.33%, compared with diesel at full engine load.

(2) With increase in ethanol addition, the cylinder pressure and temperature are reduced. It is due to the lower heating value of ethanol. Specifically, the maximum cylinder pressure value and cylinder temperature reduction were observed in BE20 for 4.31% and BE15 for 1.23% compared with biodiesel, at full engine load.

(3) Ethanol added to biodiesel can significantly decrease NOx, CO, and soot emissions compared with biodiesel. Specifically, the maximum reduction of NOx and CO emissions are 29.32% and 39.57% in BE20 at full engine load. Compared with biodiesel, the soot emission is reduced by 7.06%.

In general, ethanol added to biodiesel can significantly improve engine combustion and emission characteristics compared with pure biodiesel. According to the engine performance, combustion, and emission characteristics, the best addition ratio is BE20. Therefore, ethanol plays an important role.

Author Contributions: Data curation, Y.Z. (Yunhao Zhong), Y.Z. (Yanhui Zhang), C.M., and A.U.; formal analysis, C.M.; investigation, C.M., and A.U.; methodology, Y.Z. (Yanhui Zhang); project administration, Y.Z. (Yunhao Zhong); software, A.U.; writing—original draft, Y.Z. (Yanhui Zhang), Y.Z. (Yunhao Zhong), C.M., and A.U.; writing—review and editing, Y.Z. (Yanhui Zhang), Y.Z. (Yunhao Zhong) and C.M. All authors have read and agreed to the published version of the manuscript.

Funding: This work is supported by the Natural Science Foundation of Guangxi under the research grants AA18242036-2, 2018GXNSFAA281267 and 2018GXNSFAA294122; this research is supported by the Innovation Project of Guangxi University of Science and Technology Graduate Education under the research grants of GKYC202202.

Institutional Review Board Statement: Not applicable.

Informed Consent Statement: Not applicable.

Data Availability Statement: All data used to support the findings of this study are included within the article.

Conflicts of Interest: The authors declare that they have no known competing financial interests or personal relationships that could have appeared to influence the work reported in this paper.

References

1. Zhang, Z.; Tian, J.; Xie, G.; Li, J.; Xu, W.; Jiang, F.; Huang, Y.; Tan, D. Investigation on the combustion and emission characteristics of diesel engine fueled with diesel/methanol/n-butanol blends. *Fuel* **2022**, *314*, 123088. [CrossRef]
2. Xie, B.; Peng, Q.; Yang, W.; Li, S.; E, J.; Li, Z.; Tao, M.; Zhang, A. Effect of pins and exit-step on thermal performance and energy efficiency of hydrogen-fueled combustion for micro-thermophotovoltaic. *Energy* **2022**, *239*, 122341. [CrossRef]
3. Zhong, W.; Mahmoud, N.; Wang, Q. Experimental and modeling study of the autoignition characteristics of gasoline/hydrogenated catalytic biodiesel blends over low-to-intermediate temperature. *Fuel* **2022**, *313*, 122919. [CrossRef]
4. Zhong, W.; Mahmoud, N.; Wang, Q. Numerical study of spray combustion and soot emission of gasoline–biodiesel fuel under gasoline compression ignition-relevant conditions. *Fuel* **2022**, *310*, 122293. [CrossRef]
5. Zhang, Z.; E, J.; Deng, Y.; Pham, M.; Zuo, W.; Peng, Q.; Yin, Z. Effects of fatty acid methyl esters proportion on combustion and emission characteristics of a biodiesel fueled diesel engine. *Energy Convers. Manag.* **2018**, *159*, 244–253. [CrossRef]
6. Zhang, Z.; E, J.; Chen, J.; Zhu, H.; Zhao, X.; Han, D.; Zuo, W.; Peng, Q.; Gong, J.; Yin, Z. Effects of low-level water addition on spray, combustion and emission characteristics of a medium speed diesel engine fueled with biodiesel fuel. *Fuel* **2019**, *239*, 245–262. [CrossRef]
7. E, J.; Zhang, Z.; Chen, J.; Pham, M.; Zhao, X.; Peng, Q.; Zhang, B.; Yin, Z. Performance and emission evaluation of a marine diesel engine fueled by water biodiesel-diesel emulsion blends with a fuel additive of a cerium oxide nanoparticle. *Energy Convers. Manag.* **2018**, *169*, 194–205. [CrossRef]
8. Zhong, W.; Pachiannan, T.; He, Z.; Xuan, T.; Wang, Q. Experimental study of ignition, lift-off length and emission characteristics of diesel/hydrogenated catalytic biodiesel blends. *Appl. Energy* **2019**, *235*, 641–652. [CrossRef]
9. Peng, Q.; Xie, B.; Yang, W.; Tang, S.; Li, Z.; Zhou, P.; Luo, N. Effects of porosity and multilayers of porous medium on the hy-drogen-fueled combustion and micro-thermophotovoltaic. *Renew. Energy* **2021**, *174*, 391–402. [CrossRef]
10. Zhang, B.; Li, X.; Zuo, Q.; Yin, Z.; Zhang, J.; Chen, W.; Lu, C.; Tan, D. Effects analysis on hydrocarbon light-off performance of a catalytic gasoline particulate filter during cold start. *Environ. Sci. Pollut. Res.* **2022**. [CrossRef]
11. Zhong, W.; He, Z.; Wang, Q.; Shao, Z.; Tao, X. Experimental study of combustion and emission characteristics of diesel engine with diesel/second-generation biodiesel blending fuels. *Energy Convers. Manag.* **2016**, *121*, 241–250. [CrossRef]
12. E, J.; Liu, G.; Zhang, Z.; Han, D.; Chen, J.; Wei, K.; Gong, J.; Yin, Z. Effect analysis on cold starting performance enhancement of a diesel engine fueled with biodiesel fuel based on an improved thermodynamic model. *Appl. Energy.* **2019**, *243*, 321–335. [CrossRef]
13. Peng, Q.; Wei, J.; Yang, W.; E, J. Study on combustion characteristic of premixed H2/C3H8/air and working performance in the micro combustor with block. *Fuel* **2022**, *318*, 123676. [CrossRef]
14. Zhang, B.; E, J.; Gong, J.; Zhao, X.; Hu, W. Influence of structural and operating factors on performance degradation of the diesel particulate filter based on composite regeneration. *Appl. Therm. Eng.* **2017**, *121*, 838–852. [CrossRef]
15. Aydin, H.; İlkılıç, C. Effect of ethanol blending with biodiesel on engine performance and exhaust emissions in a CI engine. *Appl. Therm. Eng.* **2010**, *30*, 1199–1204. [CrossRef]
16. Zhang, B.; Zuo, H.; Huang, Z.; Tan, J.; Zuo, Q. Endpoint forecast of different diesel-biodiesel soot filtration process in diesel particulate filters considering ash deposition. *Fuel* **2020**, *272*, 117678. [CrossRef]
17. Zhang, Z.; Ye, J.; Tan, D.; Feng, Z.; Luo, J.; Tan, Y.; Huang, Y. The effects of Fe2O3 based DOC and SCR catalyst on the combustion and emission characteristics of a diesel engine fueled with biodiesel. *Fuel* **2021**, *290*, 120039. [CrossRef]
18. Zhang, Z.; Ye, J.; Lv, J.; Xu, W.; Tan, D.; Jiang, F.; Huang, H. Investigation on the effects of non-uniform porosity catalyst on SCR characteristic based on the field synergy analysis. *J. Environ. Chem. Eng.* **2022**, *10*, 107056. [CrossRef]
19. Biswas, S.; Kakati, D.; Chakraborti, P.; Banerjee, R. Assessing the potential of ethanol in the transition of biodiesel combustion to RCCI regimes under varying injection phasing strategies: A performance-emission-stability and tribological perspective. *Fuel* **2021**, *304*, 121346. [CrossRef]
20. Zhu, L.; Cheung, C.S.; Zhang, W.G.; Huang, Z. Combustion, performance and emission characteristics of a DI diesel engine fueled with ethanol–biodiesel blends. *Fuel* **2011**, *90*, 1743–1750. [CrossRef]

21. Wu, G.; Ge, J.C.; Choi, N.J. Effect of Ethanol Additives on Combustion and Emissions of a Diesel Engine Fueled by Palm Oil Biodiesel at Idling Speed. *Energies* **2021**, *14*, 1428. [CrossRef]
22. Gawale, G.R.; Naga Srinivasulu, G. Experimental investigation of ethanol/diesel and ethanol/biodiesel on dual fuel mode HCCI engine for different engine load conditions. *Fuel* **2020**, *263*, 116725. [CrossRef]
23. Jiang, Z.; Gan, Y.; Ju, Y.; Liang, J.; Zhou, Y. Experimental study on the electrospray and combustion characteristics of biodiesel-ethanol blends in a meso-scale combustor. *Energy* **2019**, *179*, 843–849. [CrossRef]
24. Zhang, Z.; Lv, J.; Xie, G.; Wang, S.; Ye, Y.; Huang, G.; Tan, D. Effect of assisted hydrogen on combustion and emission characteristics of a diesel engine fueled with biodiesel. *Energy* **2022**, *254*, 124269. [CrossRef]
25. Zhang, Z.; Li, J.; Tian, J.; Zhong, Y.; Zou, Z.; Dong, R.; Gao, S.; Xu, W.; Tan, D. The effects of Mn-based catalysts on the selective catalytic reduction of NOx with NH3 at low temperature: A review. *Fuel Process. Technol.* **2022**, *230*, 107213. [CrossRef]
26. An, H.; Yang, W.M.; Li, J. Numerical modeling on a diesel engine fueled by biodiesel–methanol blends. *Energy Convers. Manag.* **2015**, *93*, 100–108. [CrossRef]
27. An, H.; Yang, W.M.; Li, J. Effects of ethanol addition on biodiesel combustion: A modeling study. *Appl. Energy.* **2015**, *143*, 176–188. [CrossRef]
28. Yilmaz, N. Performance and emission characteristics of a diesel engine fuelled with biodiesel–ethanol and biodiesel–methanol blends at elevated air temperatures. *Fuel* **2012**, *94*, 440–443. [CrossRef]
29. Datta, A.; Mandal, B.K. Engine performance, combustion and emission characteristics of a compression ignition engine operating on different biodiesel-alcohol blends. *Energy* **2017**, *125*, 470–483. [CrossRef]
30. Asadi, A.; Kadijani, O.N.; Doranehgard, M.H.; Bozorg, M.V.; Xiong, Q.; Shadloo, M.S.; Li, L.K.B. Numerical study on the application of biodiesel and bioethanol in a multiple injection diesel engine. *Renew. Energy* **2020**, *150*, 1019–1029. [CrossRef]
31. Li, J.; Zhang, Z.; Ye, Y.; Li, W.; Yuan, T.; Wang, H.; Li, Y.; Tan, D.; Zhang, C. Effects of different injection timing on the performance, combustion and emission characteristics of diesel/ethanol/n-butanol blended diesel engine based on multi-objective optimization theory. *Energy* **2022**, *260*, 125056. [CrossRef]
32. Jurić, F.; Petranović, Z.; Vujanović, M.; Katrašnik, T.; Vihar, R.; Wang, X.; Duić, N. Experimental and numerical investigation of injection timing and rail pressure impact on combustion characteristics of a diesel engine. *Energy Convers. Manag.* **2019**, *185*, 730–739. [CrossRef]
33. Zhang, Z.; Li, J.; Tian, J.; Dong, R.; Zou, Z.; Gao, S.; Tan, D. Performance, combustion and emission characteristics investigations on a diesel engine fueled with diesel/ethanol/n-butanol blends. *Energy* **2022**, *249*, 123733. [CrossRef]
34. Luo, Z.; Plomer, M.; Lu, T.; Som, S.; Longman, D.E.; Sarathy, S.M.; Pitz, W.J. A reduced mechanism for biodiesel surrogates for compression ignition engine applications. *Fuel* **2012**, *99*, 143–153. [CrossRef]
35. Li, X.; Yao, X.; Shen, T. Combustion Reaction Mechanism Construction by Two-parameter Rate Constant Method. *Chem. J. Chin. Univ.* **2020**, *41*, 512–520.
36. Shojae, K.; Mahdavian, M.; Khoshandam, B.; Karimi-Maleh, H. Improving of CI engine performance using three different types of biodiesel. *Process Saf. Environ. Prot.* **2021**, *149*, 977–993. [CrossRef]
37. Zhang, Z.; Lv, J.; Li, W.; Long, J.; Wang, S.; Tan, D.; Yin, Z. Performance and emission evaluation of a marine diesel engine fueled with natural gas ignited by biodiesel-diesel blended fuel. *Energy* **2022**, *256*, 124662. [CrossRef]
38. Shirneshan, A.; Bagherzadeh, S.A.; Najafi, G.; Mamat, R.; Mazlan, M. Optimization and investigation the effects of using biodiesel-ethanol blends on the performance and emission characteristics of a diesel engine by genetic algorithm. *Fuel* **2021**, *289*, 119753. [CrossRef]
39. Yesilyurt, M.K.; Aydin, M. Experimental investigation on the performance, combustion and exhaust emission characteristics of a compression-ignition engine fueled with cottonseed oil biodiesel/diethyl ether/diesel fuel blends. *Energy Convers. Manag.* **2020**, *205*, 112355. [CrossRef]
40. Wei, L.; Cheung, C.S.; Ning, Z. Effects of biodiesel-ethanol and biodiesel-butanol blends on the combustion, performance and emissions of a diesel engine. *Energy* **2018**, *155*, 957–970. [CrossRef]
41. Zhang, Z.; Tian, J.; Li, J.; Lv, J.; Wang, S.; Zhong, Y.; Dong, R.; Gao, S.; Cao, C.; Tan, D. Investigation on combustion, performance and emission characteristics of a diesel engine fueled with diesel/alcohol/n-butanol blended fuels. *Fuel* **2022**, *320*, 123975. [CrossRef]
42. Tutak, W.; Jamrozik, A.; Pyrc, M.; Sobiepański, M. A comparative study of co-combustion process of diesel-ethanol and biodiesel-ethanol blends in the direct injection diesel engine. *Appl. Therm. Eng.* **2017**, *117*, 155–163. [CrossRef]
43. Zuo, L.; Wang, J.; Mei, D.; Dai, S.; Adu-Mensah, D. Experimental investigation on combustion and (regulated and unregulated) emissions performance of a common-rail diesel engine using partially hydrogenated biodiesel-ethanol-diesel ternary blend. *Renew. Energy.* **2022**, *185*, 1272–1283. [CrossRef]
44. Tongroon, M.; Saisirirat, P.; Suebwong, A.; Aunchaisri, J.; Kananont, M.; Chollacoop, N. Combustion and emission characteristics investigation of diesel-ethanol-biodiesel blended fuels in a compression-ignition engine and benefit analysis. *Fuel* **2019**, *255*, 115728. [CrossRef]
45. Ma, Q.; Zhang, Q.; Zheng, Z. An experimental assessment on low temperature combustion using diesel/biodiesel/C2, C5 alcohol blends in a diesel engine. *Fuel* **2021**, *288*, 119832. [CrossRef]
46. Zhang, Q.; Chen, G.; Zheng, Z.; Liu, H.; Xu, J.; Yao, M. Combustion and emissions of 2, 5-dimethylfuran addition on a diesel engine with low temperature combustion. *Fuel* **2013**, *103*, 730–735. [CrossRef]

47. Gowrishankar, S.; Krishnasamy, A. A relative assessment of emulsification and water injection methods to mitigate higher oxides of nitrogen emissions from biodiesel fueled light-duty diesel engine. *Fuel* **2022**, *308*, 121926. [CrossRef]
48. Rajesh, K.; Natarajan, M.P.; Devan, P.K.; Ponnuvel, S. Coconut fatty acid distillate as novel feedstock for biodiesel production and its characterization as a fuel for diesel engine. *Renew. Energy* **2021**, *164*, 1424–1435. [CrossRef]
49. Qi, D.; Ma, L.; Chen, R.; Jin, X.; Xie, M. Effects of EGR rate on the combustion and emission characteristics of diesel-palm oil-ethanol ternary blends used in a CRDI diesel engine with double injection strategy. *Appl. Therm. Eng.* **2021**, *199*, 117530. [CrossRef]
50. Kodate, S.V.; Raju, P.S.; Yadav, A.K.; Kumar, G.N. Effect of fuel preheating on performance, emission and combustion characteristics of a diesel engine fuelled with Vateria indica methyl ester blends at various loads. *J. Environ. Manag.* **2022**, *304*, 114284. [CrossRef]
51. Sathish, T.; Mohanavel, V.; Arunkumar, M.; Rajan, K.; Soudagar, M.E.M.; Mujtaba, M.A.; Salmen, S.H.; Al Obaid, S.; Fayaz, H.; Sivakumar, S. Utilization of Azadirachta indica biodiesel, ethanol and diesel blends for diesel engine applications with engine emission profile. *Fuel* **2022**, *319*, 123798. [CrossRef]
52. Fan, L.; Cheng, F.; Zhang, T.; Liu, G.; Yuan, J.; Mao, P. Visible-light photoredox-promoted desilylative allylation of α-silylamines: An efficient route to synthesis of homoallylic amines. *Tetrahedron Lett.* **2021**, *81*, 153357. [CrossRef]
53. Tan, D.; Chen, Z.; Li, J.; Luo, J.; Yang, D.; Cui, S.; Zhang, Z. Effects of Swirl and Boiling Heat Transfer on the Performance Enhancement and Emission Reduction for a Medium Diesel Engine Fueled with Biodiesel. *Processes* **2021**, *9*, 568. [CrossRef]
54. Zhang, Z.; Tian, J.; Li, J.; Cao, C.; Wang, S.; Lv, J.; Zheng, W.; Tan, D. The development of diesel oxidation catalysts and the effect of sulfur dioxide on catalysts of metal-based diesel oxidation catalysts: A review. *Fuel Process. Technol.* **2022**, *233*, 107317.